Synthetic Aperture Radar Imaging with Motion Estimation and Autofocus

L. Borcea[1], T. Callaghan[1], G. Papanicolaou[3]

[1]Computational and Applied Mathematics, Rice University,
MS 134, 6100 Main St. Houston, TX 77005-1892, USA
[3] Department of Mathematics, Stanford University, Stanford CA 94305, USA

E-mail: borcea@rice.edu, tscallaghan@rice.edu, and papanicolaou@stanford.edu

Abstract. We introduce from first principles a synthetic aperture radar (SAR) imaging and target motion estimation method that is combined with compensation for radar platform trajectory perturbations. The main steps of the method are (a) segmentation of the data into properly calibrated small apertures, (b) motion or platform trajectory perturbation estimation using the Wigner transform and the ambiguity function of the data, in a complementary way, (c) combination of small aperture estimates and construction of high resolution images over wide apertures. The analysis provides quantitative criteria for implementing the aperture segmentation and the parameter estimation process. X-band persistent surveillance SAR is a specific application that is covered by our analysis. Detailed numerical simulations illustrate the robust applicability of the theory and validate the theoretical resolution analysis.

1. Introduction.

In synthetic aperture radar (SAR) we want to image the reflectivity of a given surface using an antenna system mounted on a platform flying over it, as illustrated in Figure 1. Information about the unknown reflectivity is obtained by emitting periodically at rate Δs probing signals $f(t)$ and recording the echoes $D(s,t)$, indexed by the slow time s of the SAR platform displacement and the fast time t of the probing signal. The slow time parametrizes the location $\vec{\mathbf{r}}_p(s)$ of the platform at the instant it emits the signal, and the fast time t runs between two consecutive illuminations ($0 < t < \Delta s$).

An image is formed by superposing over a platform trajectory segment of arc length (aperture) a, the data $D(s,t)$ match-filtered with the time reversed emitted signal $f(t)$, and back propagated with the round trip travel times $\tau(s,\vec{\boldsymbol{\rho}}^{\,\mathcal{I}})$ from the platform to the imaging points $\vec{\boldsymbol{\rho}}^{\,\mathcal{I}}$,

$$\begin{aligned}\mathcal{I}(\vec{\boldsymbol{\rho}}^{\,\mathcal{I}}) &= \int_{-S(a)}^{S(a)} ds \int dt\, D(s,t)\overline{f\left(t-\tau(s,\vec{\boldsymbol{\rho}}^{\,\mathcal{I}})\right)} \\ &= \int_{\omega_o-\pi B}^{\omega_o+\pi B} \frac{d\omega}{2\pi} \int_{-S(a)}^{S(a)} ds\, \overline{\widehat{f}(\omega)}\widehat{D}(s,\omega)e^{-i\omega\tau(s,\vec{\boldsymbol{\rho}}^{\,\mathcal{I}})}. \end{aligned} \tag{1.1}$$

Here hat denotes Fourier transform, the bar stands for complex conjugate, B and ω_o are the bandwidth and central frequency of $f(t)$ respectively, $S(a)$ is the slow time range over the aperture of length a, and

$$\tau(s,\vec{\boldsymbol{\rho}}^{\,\mathcal{I}}) = 2|\vec{\mathbf{r}}_p(s) - \vec{\boldsymbol{\rho}}^{\,\mathcal{I}}|/c \tag{1.2}$$

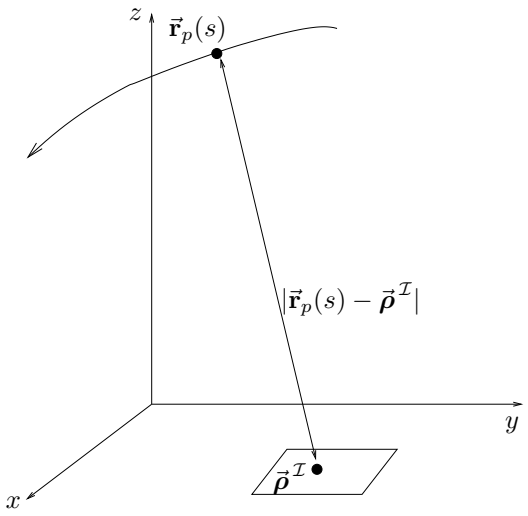

Figure 1. Setup for synthetic aperture imaging.

is the round trip travel time from the platform to the imaging point $\vec{\boldsymbol{\rho}}^{\mathcal{I}}$. See Figure 1 for an illustration of the imaging setup.

The basic theory of SAR imaging is presented in [9, 13, 8]. The imaging function (1.1) can be modified in the case of large apertures by introducing a weight factor $W(s)$ that accounts for the geometrical spreading of the wave field over the length of the aperture

$$\mathcal{I}_W(\vec{\boldsymbol{\rho}}^{\mathcal{I}}) = \int_{\omega_o-\pi B}^{\omega_o+\pi B} \frac{d\omega}{2\pi} \int_{-S(a)}^{S(a)} ds\, W(s) \overline{\widehat{f}(\omega)} \widehat{D}(s,\omega) e^{-i\omega\tau(s,\vec{\boldsymbol{\rho}}^{\mathcal{I}})}. \tag{1.3}$$

The weight factor is often approximated by $W(s) \approx |\vec{\mathbf{r}}_p(s) - \vec{\boldsymbol{\rho}}^{\mathcal{I}}|$. It can be calculated exactly in the case of simple platform trajectories, so that the point spread function is as tight as possible [6, 15, 9].

Our main objective in this paper is to image moving localized reflectors, or targets, that can be tracked in real time by processing data over sufficiently small sub-apertures. We introduce a process based on the Wigner transform and the ambiguity function of properly segmented small aperture data, that can either estimate the target motion or compensate the SAR platform trajectory perturbation. The latter process is called *autofocus*. It is only after the motion estimation and autofocus have been carried out over successive, overlapping segments of the trajectory, that we can compute the final image over an extended aperture, using an imaging function like (1.3). This approach can be applied to a wide range of SAR imaging systems, including X-band persistent surveillance SAR.

The main steps in the analysis of SAR imaging with motion estimation and autofocus are as follows. First we segment the data into small apertures and find analytically under what conditions phases can be linearized so that computationally efficient local Fourier transforms can be used. Next we describe an approach that estimates incremental target motion relative to the SAR platform, using the location in the phase space of the peaks of the Wigner transform and the ambiguity function of the data. Moreover, we show that the Wigner transform and the ambiguity function provide complementary information and that they have different resolution. Most of the analysis assumes data in a time window containing the echoes from a single strong target, but we consider the case of multiple targets, as well.

Note that it is only the relative motion between the target and the SAR platform that appears in the

problem. Thus, when imaging a single strong target, we cannot estimate simultaneously its speed and the platform trajectory perturbations. To decouple the motion estimation from the autofocus process we need a complex imaging scene, with multiple targets that move at different speeds. We consider in this paper the case of multiple strong stationary targets, and show under which conditions we can carry the autofocus process. Because the Wigner transform and the ambiguity function have multiple peaks in this case, we use their centroids[2, 3] to estimate the platform trajectory perturbations. The results extend easily to multiple targets that move in the same way, as a group. The case of multiple targets in different motion is not discussed here, because the phase space approach alone does not work. It must be complemented with a data pre-processing (filtering) step that will be presented in a different paper.

That the Wigner transform is a natural tool for detection and imaging of moving targets has been known. For example, the estimation of target motion from the peaks of the Wigner transform is considered in [11, 10]. The robustness of the estimation to additive noise and extensions to cases with few targets are addressed in [3]. See also [16, 17] for experimental results. Alternative approaches to autofocus are given in [14, 12, 4]. The main result of this paper is the theory of estimating target motion and compensating for platform trajectory perturbation using in a complementary way the Wigner transform and the ambiguity function. It includes the analysis of robustness to uncertainty of the flight path and of the initial target locations.

The paper is organized as follows. We begin in Section 2 with a mathematical model of the SAR data and the range compression processing. The first appendix provides a summary of the relevant physical parameters that are typical in X-band persistent surveillance SAR. In Section 3 we carry out a target motion estimation using the Wigner transform and the ambiguity function of the range compressed data. In Section 4 we apply the results to the autofocus problem. These two sections show how by identifying the peaks in the Wigner transform and ambiguity function we can estimate parameters that can be used for either improving target motion estimation or for compensation for SAR platform trajectory perturbations. The case of multiple stationary targets is considered in Section 5. In Section 6 we present the results of detailed numerical simulations, first for target motion estimation alone, and then for autofocus, without target motion. The latter include results for multiple targets. We end with a summary in Section 7.

2. Mathematical model of the data.

To study the resolution of motion estimation and autofocus with phase space methods based on Wigner transforms and ambiguity functions, we use a simple model of the SAR data. It corresponds to the reflectivity $\mathcal{R}(t, \mathbf{x})$ of a small (point-like) moving target. The target trajectory is an arbitrary curve in the imaging surface $\vec{\mathbf{x}} = (\mathbf{x}, z = h(\mathbf{x}))$, with elevation $z = h(\mathbf{x})$. We suppose that it is smooth enough to approximate the motion locally, between two consecutive illuminations $t \in (0, \Delta s)$, by translation from $\vec{\boldsymbol{\rho}}(s) = (\boldsymbol{\rho}(s), h(\boldsymbol{\rho}(s))$, at speed

$$\vec{\mathbf{u}}(s) = (\mathbf{u}(s), \nabla h(\boldsymbol{\rho}(s)) \cdot \mathbf{u}(s)) \tag{2.1}$$

on the imaging surface. For simplicity of the exposition, we take a flat surface $z = h(\mathbf{x}) = 0$, so that $\vec{\mathbf{u}}(s) = (\mathbf{u}(s), 0)$ and we can write

$$\mathcal{R}(t, \mathbf{x}) = \delta(\mathbf{x} - \boldsymbol{\rho}(s) - t\mathbf{u}(s)), \qquad t \in (0, \Delta s). \tag{2.2}$$

The results extend easily to surfaces with known elevation $z = h(\mathbf{x})$ and speed (2.1).

Our analysis is based on several approximations that are motivated by specific SAR data regimes. One such regime arises in the GOTCHA Volumetric SAR Data Set [7] for X-band persistent surveillance SAR, described in Appendix A, and used as an illustration throughout the paper.

2.1. ***The basic data model and range compression.***

We assume hereafter that $\vec{\mathbf{u}}(s)$ and the platform speed

$$\vec{\mathbf{V}}(s) = \vec{\mathbf{r}}_p'(s) = V(s)\vec{\mathbf{t}}(s) \tag{2.3}$$

satisfy

$$|\vec{\mathbf{u}}(s)| \lesssim V(s) \quad \text{and} \quad \frac{\omega_o}{c} V(s)\, \tau(s, \vec{\boldsymbol{\rho}}(s)) = 2\pi \frac{V(s)\, \tau(s, \vec{\boldsymbol{\rho}}(s))}{\lambda_o} \sim 1. \tag{2.4}$$

This says that we are in a high frequency regime, where the platform moves a distance comparable to λ_o over the very short travel time duration $\tau(s, \vec{\boldsymbol{\rho}}(s))$, at speed of light c. The platform speed is along the unit vector $\vec{\mathbf{t}}(s)$, tangential to the trajectory at $\vec{\mathbf{r}}_p(s)$. The range scale L gives the typical distance from the SAR platform to the imaging scene and we suppose that it is similar to the radius $R(s)$ of curvature of the platform trajectory. We also assume a relatively narrow bandwidth B, satisfying

$$\frac{V(s)}{c} \ll \frac{B}{\nu_o} \ll 1. \tag{2.5}$$

The bandwidth is narrow ($B \ll \nu_o$), but B is sufficiently large so that over the duration $O(1/B)$ of the range compressed signal, the platform moves a small distance with respect to λ_o. The following model of the data $D(s,t)$ is derived in Appendix B.

Proposition 1. *Let $f(t) = e^{-i\omega_o t} f_B(t)$ be the probing signal, given by a base-band waveform $f_B(t)$ modulated by a carrier frequency $\nu_o = \omega_o/(2\pi)$. We have*

$$\widehat{D}(s,\omega) = \int dt\, e^{i\omega t} D(s,t) \approx \frac{(\omega_o/c)^2 \widehat{f}_B(\omega - \omega_o)}{(4\pi|\vec{\mathbf{r}}_p(s) - \vec{\boldsymbol{\rho}}(s)|)^2} e^{i\omega_o \psi(s) + i\omega\tau(s,\vec{\boldsymbol{\rho}}(s))}, \tag{2.6}$$

where $\psi(s)$ is the Doppler phase

$$\psi(s) = \tau(s, \vec{\boldsymbol{\rho}}(s)) \left(\frac{\vec{\mathbf{V}}(s)}{c} - \frac{\vec{\mathbf{u}}(s)}{c} \right) \cdot \vec{\mathbf{m}}(s), \qquad \vec{\mathbf{m}}(s) = \frac{\vec{\mathbf{r}}_p(s) - \vec{\boldsymbol{\rho}}(s)}{|\vec{\mathbf{r}}_p(s) - \vec{\boldsymbol{\rho}}(s)|}. \tag{2.7}$$

Instead of working directly with the recorded data $D(s,t)$, we compress them by convolution with the complex conjugate of the time reversed emitted pulse $f(-t)$, offset by the travel time $\tau(s, \vec{\boldsymbol{\rho}}_o)$ to a reference point $\vec{\boldsymbol{\rho}}_o$ in the imaging plane,

$$D_r(s,t) = \int dt'\, D(s,t') \overline{f\,(t' - t - \tau(s, \vec{\boldsymbol{\rho}}_o))}, \qquad |\vec{\boldsymbol{\rho}}(s) - \vec{\boldsymbol{\rho}}_o| \ll L. \tag{2.8}$$

We shall make the approximation

$$|\widehat{f}_B(\omega - \omega_o)| \approx |\widehat{f}_B(0)| 1_{[\omega_o, \pi B]}(\omega), \tag{2.9}$$

where $1_{[\omega_o,\pi B]}(\omega)$ is the indicator function of interval $[\omega_o - \pi B, \omega_o + \pi B]$. This holds for linear frequency modulated chirps [13] or for pulses $f(t) \sim e^{-i\omega_o t}\mathrm{sinc}(\pi B t)$. We also set the Doppler phase $\psi(s)$ to the constant $\psi(0)$ over the small apertures a used in our data processing, because for $|s| \leq S(a) = a/(2V)$, we suppose

$$\omega_o\, [\psi(s) - \psi(0)] \sim \omega_o s\, \psi'(0) \sim \frac{\omega_o s V^2}{c^2} \sim \frac{aV}{\lambda_o c} \ll 1. \tag{2.10}$$

The model of the range compressed data follows from (2.6), (2.8) and (2.9),

$$\widehat{D}_r(s,\omega) \approx \frac{\omega_o^2}{c^2} \frac{\left|\widehat{f}_B(0)\right|^2 1_{[\omega_o,\pi B]}(\omega)}{(4\pi|\vec{\mathbf{r}}_p(s)-\vec{\boldsymbol{\rho}}(s)|)^2} \exp\left\{i\omega_o\psi(0) + i\omega\left[\tau(s,\vec{\boldsymbol{\rho}}(s)) - \tau(s,\vec{\boldsymbol{\rho}}_o)\right]\right\}. \tag{2.11}$$

It has the advantage that no matter how long is the waveform $f(t)$, $D_r(s,t)$ behaves like a short pulse with support $O(1/B)$. Another advantage is that since $\widehat{D}_r(s,\omega)$ has smaller phases than $\widehat{D}(s,\omega)$, it is more convenient in numerical computations.

Remark 1. *In the GOTCHA Volumetric SAR data set described in Appendix A, the assumptions above are justified as follows. Apertures $a = 124m$, of one degree on the circular planar path of the platform, with radius $R = 7.1km$, are spanned by the aircraft at speed $V = 250km/h \approx 70m/s$ in $1.8s$. In such short time, the target motion can be approximated by translation at speed $|\vec{\mathbf{u}}| \sim 100km/h \approx 28m/s \lesssim V$. This gives $2\pi\tau V = 2.9cm$, which is similar to $\lambda_o = 3cm$, so (2.4) holds. Moreover, $|\vec{\mathbf{V}}|/c = 2.3\cdot 10^{-7} \ll B/\nu_0 = 6.5\cdot 10^{-2}$, so (2.5) holds. The target range is $L \sim 10km$, which is similar to R, and $aV/(\lambda_o c) = 9.6\cdot 10^{-4} \ll 1$, so (2.10) holds.*

3. Motion Estimation with the Wigner transform and ambiguity function.

We describe a phase space approach to target motion estimation. It is based on the Wigner transform and the ambiguity function of the data over small sub-apertures. We give quantitative criteria for the aperture segmentation, and explain how the Wigner transform and the ambiguity function give complementary information about the target motion. We also compare their resolution, and study their robustness to uncertainty of the flight path and of the initial target location.

We assume hereafter that the platform speed $V(s) = |\vec{\mathbf{V}}(s)|$ along the tangent $\vec{\mathbf{t}}(s)$ of the flight path, the curvature $R(s)$ and the target speed $\vec{\mathbf{u}}(s) = (\mathbf{u}(s), 0)$ are sufficiently smooth functions of s, to approximate them by constants over the short time intervals that define the sub-apertures. We also introduce the notation $u = |\vec{\mathbf{u}}|$.

3.1. ***Motion estimation with the Wigner transform.***

The Wigner transform of the range compressed SAR data is given by

$$\mathcal{W}(s,\Omega,\omega,T) = \int_{-\tilde{\Omega}}^{\tilde{\Omega}} d\tilde{\omega} \int_{-\tilde{S}}^{\tilde{S}} d\tilde{s}\, \widehat{D}_r\left(s+\frac{\tilde{s}}{2},\omega+\frac{\tilde{\omega}}{2}\right) \overline{\widehat{D}_r\left(s-\frac{\tilde{s}}{2},\omega-\frac{\tilde{\omega}}{2}\right)} e^{i\tilde{s}\Omega - i\tilde{\omega}T}, \tag{3.1}$$

where Ω and T are frequency and time variables, dual to the variables of integration $\tilde{s}$ and $\tilde{\omega}$. The $\tilde{\omega}$ integral limit is $\tilde{\Omega} = 2\pi B - 2|\omega-\omega_o|$, so that $\omega \pm \tilde{\omega}/2$ remains in the support of $\widehat{D}_r$ for all $\tilde{\omega} \in [-\tilde{\Omega},\tilde{\Omega}]$. The time offset interval $\tilde{s} \in [-\tilde{S},\tilde{S}]$ is chosen in terms of an aperture a measured along the trajectory, $\tilde{S} = a/(2V)$. The center of the aperture is indexed by the slow time s.

The Wigner transform takes the following form, as proved in Appendix C.

Proposition 2. *Consider apertures a so that the Fresnel number $a^2/(\lambda_o L)$ satisfies*

$$\frac{a^2}{\lambda_o L} \ll \frac{4\nu_o V}{Bu}, \quad \text{and} \quad \frac{a^2}{\lambda_o L} \ll \frac{8LV}{au}. \tag{3.2}$$

Then, the Wigner transform evaluated at $\omega = \omega_o$ has the form

$$\mathcal{W}(s,\Omega,\omega_o,T) \sim \frac{|\widehat{f}_B(0)|^4}{|\vec{\mathbf{r}}_p(s)-\vec{\boldsymbol{\rho}}(s)|^4} sinc\{\pi B\left[T-\Delta\tau(s)\right]\} sinc\left\{\frac{4\pi a}{\lambda_o}\left[\frac{\Omega c}{2\omega_o V} - \Phi(s)\right]\right\}, \tag{3.3}$$

where

$$\Delta\tau(s) = \tau(s, \vec{\boldsymbol{\rho}}(s)) - \tau(s, \vec{\boldsymbol{\rho}}_o) \quad \textit{and} \quad \Phi(s) = \frac{\vec{\mathbf{u}}}{V} \cdot \vec{\mathbf{m}}(s) - \vec{\mathbf{t}}(s) \cdot (\vec{\mathbf{m}}(s) - \vec{\mathbf{m}}_o(s))\,. \tag{3.4}$$

Here, symbol $\sim$ *stands for approximate, up to a multiplicative constant,* $\vec{\mathbf{m}}(s)$ *is the unit vector in (2.7), and*

$$\vec{\mathbf{m}}_o(s) = \frac{\vec{\mathbf{r}}_p(s) - \vec{\boldsymbol{\rho}}_o}{|\vec{\mathbf{r}}_p(s) - \vec{\boldsymbol{\rho}}_o|} \tag{3.5}$$

is the unit vector from the platform to the reference point $\vec{\boldsymbol{\rho}}_o$ *in the imaging plane.*

Remark 2. *Among the two conditions on the Fresnel number in (3.2), the first one is more restrictive, because typically* $\frac{L}{a} \gtrsim \frac{\nu_o}{B} \gg 1$*. It allows us to linearize the phases in the integral over* $\tilde{s}$ *and obtain therefore a simple expression of the Wigner transform* $\mathcal{W}$*. If we relaxed the condition to*

$$\frac{a^2}{\lambda_o L} \lesssim \frac{4\nu_o V}{Bu}, \tag{3.6}$$

we would get a more complicated formula for $\mathcal{W}$*, involving Fresnel integrals instead of the sinc functions. However, the conclusions drawn below remain similar, because they use estimates of the peaks* $\Omega^{\mathcal{W}}(s)$ *and* $T^{\mathcal{W}}(s)$ *of* $\mathcal{W}$*. These peaks are not affected by the quadratic phases in the Fresnel integrals. In GOTCHA, the second condition in (3.2) says* $a \ll 390m$ *for* $u = 100km/h$*. The relaxed condition (3.6) says* $a \lesssim 219m$*, so we can work with* $a \sim 100m$*.*

Now let us use (3.3) to relate the peaks $\Omega^{\mathcal{W}}(s)$ and $T^{\mathcal{W}}(s)$ of $\mathcal{W}$ to the travel time $\tau(s, \vec{\boldsymbol{\rho}}(s))$ and the target speed $\vec{\mathbf{u}}$ projected along $\vec{\mathbf{m}}(s)$,

$$\frac{\vec{\mathbf{u}}}{V} \cdot \vec{\mathbf{m}}(s) = \frac{c\,\Omega^{\mathcal{W}}(s)}{2\omega_o V} + \vec{\mathbf{t}}(s) \cdot (\vec{\mathbf{m}}(s) - \vec{\mathbf{m}}_o(s)) + O\left(\frac{\lambda_o}{a}\right), \tag{3.7}$$

and

$$\tau(s, \vec{\boldsymbol{\rho}}(s)) = T^{\mathcal{W}}(s) + \tau(s, \vec{\boldsymbol{\rho}}_o) + O\left(\frac{1}{B}\right). \tag{3.8}$$

Thus, we can use the peak $T^{\mathcal{W}}$ to estimate the travel time, and therefore the distance to the target. There is only one peak if there is only one target. In general, there will be many peaks, associated to different targets [3], and the Wigner transform may be used to select a time window containing the echo from a single target that we track. This assumes a separation in range between the target and the remainder of the imaging scene. The analysis in this section is based on this assumption, but we address in Section 5 the case of multiple strong targets whose pulse compressed echoes arrive at almost the same time.

To estimate $\vec{\mathbf{u}}$, we need an initial estimate of the target location in the sub-aperture. This estimate is then adjusted from one sub-aperture to another, using the estimated speed. To simplify the formulas, we assume in the analysis an estimate of $\vec{\boldsymbol{\rho}}(s)$ (i.e. of $\vec{\mathbf{m}}(s)$) at time s corresponding to the middle of the sub-aperture. The results can be obviously modified to initial location estimates by letting $\vec{\boldsymbol{\rho}}(s) \rightsquigarrow \vec{\boldsymbol{\rho}}(s) - \vec{\mathbf{u}}\,\tilde{S}/2$.

Equation (3.7) determines only one component of $\vec{\mathbf{u}}$, along $\vec{\mathbf{m}}(s)$. To get $\vec{\mathbf{u}} = (\mathbf{u}, 0)$, we also need its cross-range projection $\mathbb{P}(s)\vec{\mathbf{u}}$, where $\mathbb{P}(s)$ is the orthogonal projection

$$\mathbb{P}(s) = I - \vec{\mathbf{m}}(s)\vec{\mathbf{m}}(s)^T. \tag{3.9}$$

The latter can be determined, in principle, from additional sub-apertures with centers slightly shifted at $s + \delta_s$, by small δ_s. For example, we could use the estimated $\vec{\mathbf{u}} \cdot \vec{\mathbf{m}}(s + \delta_s)$ and $\vec{\mathbf{u}} \cdot \vec{\mathbf{m}}(s)$ to write

$$\vec{\mathbf{u}} \cdot [\vec{\mathbf{m}}(s + \delta_s) - \vec{\mathbf{m}}(s)] \approx \delta_s \vec{\mathbf{u}} \cdot \vec{\mathbf{m}}'(s) = \delta_s \frac{\left(V\vec{\mathbf{t}}(s) - \vec{\mathbf{u}}\right)}{|\vec{\mathbf{r}}_p(s) - \vec{\boldsymbol{\rho}}(s)|} \cdot \mathbb{P}(s)\vec{\mathbf{u}}.$$

However, such differentiation will not work well with noisy data. We show next that the ambiguity function complements the Wigner transform, as it provides a more robust and direct estimate of $\mathbb{P}(s)\vec{\mathbf{u}}$.

3.2. ***Motion estimation with the ambiguity function.***

The ambiguity function of the range compressed SAR data is given by

$$\mathcal{A}(s,\Omega,\tilde{s},T)=\int_{\omega_o-\pi B}^{\omega_o+\pi B}d\omega\int_{-\overline{S}}^{\overline{S}}d\overline{s}\,\widehat{D}_r\left(s+\overline{s}+\frac{\tilde{s}}{2},\omega\right)\overline{\widehat{D}_r\left(s+\overline{s}-\frac{\tilde{s}}{2},\omega\right)}e^{i\overline{s}\Omega-i(\omega-\omega_o)T}. \tag{3.10}$$

The slow time window center s and the offset $\tilde{s}$ are independent variables, and Ω and T are the dual variables of $\overline{s}$ and $\omega-\omega_o$, respectively. The expression of (3.10), in our setup, is given in the next proposition. Its derivation is very similar to that of the Wigner transform, and we do not repeat it here.

Proposition 3. *If we choose $\overline{S}=a/(2V)$, with a satisfying (3.2), the ambiguity function evaluated at $\tilde{s}=a/(2V)$ is given approximately by*

$$\mathcal{A}\left(s,\Omega,\frac{a}{2V},T\right)\sim\frac{|\widehat{f}_B(0)|^4e^{-\frac{i\omega_o a}{c}\Phi(s)}}{|\vec{\mathbf{r}}_p(s)-\vec{\boldsymbol{\rho}}_\star|^4}sinc\left\{\frac{\pi Ba}{c}\left[\frac{cT}{a}+\Phi(s)\right]\right\}sinc\left[\frac{a\Omega}{2V}+\frac{\pi a^2\Phi^\perp(s)}{\lambda_o|\vec{\mathbf{r}}_p(s)-\vec{\boldsymbol{\rho}}(s)|}\right], \tag{3.11}$$

where $\sim$ denotes approximate up to a multiplicative constant, $\Phi(s)$ is the same as in (3.4),

$$\Phi^\perp(s)=\left|\mathbb{P}(s)\left(\vec{\mathbf{t}}(s)-\frac{\vec{\mathbf{u}}}{V}\right)\right|^2-|\vec{\mathbf{r}}_p(s)-\vec{\boldsymbol{\rho}}(s)|\left[\frac{\left|\mathbb{P}_o(s)\vec{\mathbf{t}}(s)\right|^2}{|\vec{\mathbf{r}}_p(s)-\vec{\boldsymbol{\rho}}_o|}-\frac{\vec{\mathbf{t}}'(s)}{V}\cdot(\vec{\mathbf{m}}(s)-\vec{\mathbf{m}}_o(s))\right], \tag{3.12}$$

and $\mathbb{P}_o(s)$ is the orthogonal projection $\mathbb{P}_o(s)=I-\vec{\mathbf{m}}_o(s)\vec{\mathbf{m}}_o(s)^T$.

Thus, the ambiguity function allows us to estimate both the projection of $\vec{\mathbf{u}}$ on $\vec{\mathbf{m}}(s)$, and the norm of the projection of the relative speed $\vec{\mathbf{V}}-\vec{\mathbf{u}}$ on the plane orthogonal to $\vec{\mathbf{m}}(s)$. As already noted, in (3.11) we evaluate the ambiguity function at the extreme value of the slow time offset $\tilde{s}=a/(2V)$. This is to get the tightest second sinc function, which gives the sharpest estimate of the peak $\Omega^{\mathcal{A}}(s)$ in Ω.

The peak $T^{\mathcal{A}}$ of the ambiguity function determines

$$\frac{\vec{\mathbf{u}}}{V}\cdot\vec{\mathbf{m}}(s)=-\frac{cT^{\mathcal{A}}(s)}{2\tilde{S}V}+\vec{\mathbf{t}}(s)\cdot(\vec{\mathbf{m}}(s)-\vec{\mathbf{m}}_o(s))+O\left(\frac{c}{Ba}\right). \tag{3.13}$$

We already have the estimate (3.7) of $\vec{\mathbf{u}}\cdot\vec{\mathbf{m}}(s)$, from the Wigner transform. In fact, estimate (3.13) is less precise, with resolution

$$\frac{c}{Ba}=\frac{\nu_o\lambda_o}{Ba}\gg\frac{\lambda_o}{a}.$$

It is the other peak of $\mathcal{A}$ that gives the complementary information,

$$\begin{aligned}\left|\mathbb{P}(s)\left(\vec{\mathbf{t}}(s)-\frac{\vec{\mathbf{u}}}{V}\right)\right|^2 &= \left|\mathbb{P}_o(s)\vec{\mathbf{t}}(s)\right|^2\frac{|\vec{\mathbf{r}}_p(s)-\vec{\boldsymbol{\rho}}(s)|}{|\vec{\mathbf{r}}_p(s)-\vec{\boldsymbol{\rho}}_o|}+\frac{|\vec{\mathbf{r}}_p(s)-\vec{\boldsymbol{\rho}}(s)|}{V}\times\\ &\left[\vec{\mathbf{t}}'(s)\cdot(\vec{\mathbf{m}}_o(s)-\vec{\mathbf{m}}(s))-\frac{\Omega^{\mathcal{A}}(s)c}{2\omega_o\tilde{s}V}\right]+O\left(\frac{\lambda_oL}{a^2}\right),\end{aligned} \tag{3.14}$$

without any need to differentiate, as was the case with the Wigner transform. This equation, in conjunction with (3.7), determine the target speed $\mathbf{u}$, up to an ambiguity of the orientation of $\mathbf{t}-\mathbf{u}/V$ in the direction orthogonal to $\mathbf{m}$ in the imaging plane. Here $\vec{\mathbf{t}}=(\mathbf{t},t_z)$ and $\vec{\mathbf{m}}=(\mathbf{m},m_z)$.

Remark 3. *Note that because of our aperture limitation assumption (3.6), the estimate (3.14) is useful if we have a large Fresnel number*

$$1 \ll \frac{a^2}{\lambda_o L} \lesssim \frac{4\nu_o V}{Bu}. \tag{3.15}$$

This means that the aperture a cannot be too small if the motion estimation is to work. It must be large enough, but still limited by (3.6). For example, in GOTCHA, the Fresnel number is $a^2/(\lambda_o L) = 49$ *for one degree aperture, and* $4\nu_o V/(Bu) = 154$.

3.3. ***Sensitivity of target motion estimation to knowledge of its initial location.***

The estimation of $\vec{\mathbf{u}}$ requires the vector $\vec{\mathbf{m}}(s)$ in (2.7), and the target range $|\vec{\mathbf{r}}_p(s) - \vec{\boldsymbol{\rho}}(s)|$. Neglecting the SAR platform trajectory perturbations, the range is determined with resolution c/B from the travel time $\tau(s, \vec{\boldsymbol{\rho}}(s))$, which is estimated from the Wigner transform. The target location cannot be determined directly from the data, before forming an image, but we suppose that we know an estimate $\vec{\boldsymbol{\rho}}_e$ of $\vec{\boldsymbol{\rho}}(s)$, either from direct observations, or from tracking the target at previous times. That is, we approximate $\vec{\mathbf{m}}(s)$ by

$$\vec{\mathbf{m}}_e(s) = \frac{\vec{\mathbf{r}}_p(s) - \vec{\boldsymbol{\rho}}_e(s)}{|\vec{\mathbf{r}}_p(s) - \vec{\boldsymbol{\rho}}_e(s)|},$$

with $\vec{\boldsymbol{\rho}}_e$ in the imaging plane, at distance $c/2\tau(s, \vec{\boldsymbol{\rho}}(s))$ from $\vec{\mathbf{r}}_p(s)$.

Now we quantify the sensitivity of motion estimation to the error $\vec{\boldsymbol{\rho}} - \vec{\boldsymbol{\rho}}_e$. Let $\Delta\vec{\mathbf{u}} = (\Delta\mathbf{u}, 0)$ be the error of the estimated velocity. We obtain from (3.7) that

$$\frac{(\vec{\mathbf{u}} + \Delta\vec{\mathbf{u}})}{V} \cdot \vec{\mathbf{m}}^e = \frac{c\Omega^{\mathcal{W}}}{2\omega_o V} + \vec{\mathbf{t}} \cdot (\vec{\mathbf{m}}_e - \vec{\mathbf{m}}_o) = \frac{\vec{\mathbf{u}}}{V} \cdot \vec{\mathbf{m}}^e + \left(\vec{\mathbf{t}} - \frac{\vec{\mathbf{u}}}{V}\right) \cdot (\vec{\mathbf{m}}_e - \vec{\mathbf{m}}) + O\left(\frac{\lambda_o}{a}\right)$$

and therefore

$$\frac{\Delta\vec{\mathbf{u}}}{V} \cdot \vec{\mathbf{m}}_e = \left(\vec{\mathbf{t}} - \frac{\vec{\mathbf{u}}}{V}\right) \cdot (\vec{\mathbf{m}}_e - \vec{\mathbf{m}}) + O\left(\frac{\lambda_o}{a}\right) = O\left(\frac{|\vec{\boldsymbol{\rho}} - \vec{\boldsymbol{\rho}}_e|}{L}\right) + O\left(\frac{\lambda_o}{a}\right). \tag{3.16}$$

From (3.14) we have

$$\begin{aligned}\left|\mathbb{P}_e\left(\vec{\mathbf{t}} - \frac{\vec{\mathbf{u}} + \Delta\vec{\mathbf{u}}}{V}\right)\right|^2 - \left|\mathbb{P}\left(\vec{\mathbf{t}} - \frac{\vec{\mathbf{u}}}{V}\right)\right|^2 &= \frac{|\vec{\mathbf{r}}_p - \vec{\boldsymbol{\rho}}|}{V}\vec{\mathbf{t}}' \cdot (\vec{\mathbf{m}} - \vec{\mathbf{m}}_e) + O\left(\frac{\lambda_o L}{a^2} + \frac{c}{BL}\right) \\ &= O\left(\frac{|\vec{\boldsymbol{\rho}} - \vec{\boldsymbol{\rho}}_e|}{L} + \frac{\lambda_o L}{a^2}\right) = O\left(\frac{\lambda_o L}{a^2}\right),\end{aligned} \tag{3.17}$$

because $|\vec{\mathbf{t}}'| = V/R \sim V/|\vec{\mathbf{r}}_p - \vec{\boldsymbol{\rho}}|$. The second term in the error dominates the first, provided that $|\vec{\boldsymbol{\rho}} - \vec{\boldsymbol{\rho}}_e| \lesssim a$, because (3.6) and $u \lesssim V$ give

$$\frac{|\vec{\boldsymbol{\rho}} - \vec{\boldsymbol{\rho}}_e|}{L} \lesssim \frac{a}{L} \lesssim \frac{\nu_o \lambda_o}{Ba} = \frac{c}{Ba} \lesssim \frac{\lambda_o L}{a^2}.$$

We conclude from (3.17) that the cross-range velocity estimation is insensitive to the choice of the reference point $\vec{\boldsymbol{\rho}}_e$, as long as $|\vec{\boldsymbol{\rho}}_e - \vec{\boldsymbol{\rho}}| \lesssim a$. However, (3.16) shows that to maintain the resolution $\sim \lambda_o/a$ in the estimation of $\vec{\mathbf{u}} \cdot \vec{\mathbf{m}}$ with the Wigner transform, we need a more precise estimate of the target location, with $|\vec{\boldsymbol{\rho}} - \vec{\boldsymbol{\rho}}_e|$ comparable to the cross range resolution $\lambda_o L/a$.

3.4. ***Motion estimation with SAR platform trajectory perturbations.***

The SAR platform trajectory is known only approximately. We therefore consider perturbations $\vec{\boldsymbol{\mu}}(s)$ of $\vec{\mathbf{r}}_p(s)$ and set $\vec{\mathbf{r}}_p(s) \rightsquigarrow \vec{\mathbf{r}}_p(s) + \vec{\boldsymbol{\mu}}(s)$ in the data model (2.11). We assume that the SAR platform trajectory perturbations vary on the slow scale s and are small, so that only the unperturbed platform speed appears in the Doppler phase ψ in (2.7). This is because $\omega_o \psi \sim 1$ by assumption (2.4), and therefore perturbations of ψ are negligible. The effect of $\vec{\boldsymbol{\mu}}(s)$ on the amplitude of $\widehat{D}_r(s,\omega)$ is also negligible.

3.4.1. ***Assumptions about the SAR platform trajectory perturbations.*** Let us begin with the observation that the platform trajectory perturbations induce the following perturbations of the travel time

$$\frac{2}{c}|\vec{\mathbf{r}}_p(s) + \vec{\boldsymbol{\mu}}(s) - \vec{\boldsymbol{\rho}}(s)| - \tau(s, \vec{\boldsymbol{\rho}}(s)) = \frac{2}{c}\vec{\boldsymbol{\mu}}(s) \cdot \vec{\mathbf{m}}(s) + O\left(\frac{|\vec{\boldsymbol{\mu}}(s)|^2}{cL}\right), \tag{3.18}$$

with negligible residual under the assumption

$$|\vec{\boldsymbol{\mu}}(s)| \ll \sqrt{\lambda_o L}. \tag{3.19}$$

When $\vec{\mathbf{m}}(s) \cdot \vec{\boldsymbol{\mu}}(s)$ is large enough, we can estimate it directly from the perturbations of the arrival time of the pulse compressed SAR data. Since the compressed pulse support is $O(1/B)$, we can estimate and compensate $\vec{\mathbf{m}}(s) \cdot \vec{\boldsymbol{\mu}}(s)$ from the arrival times when

$$|\vec{\mathbf{m}}(s) \cdot \vec{\boldsymbol{\mu}}(s)| \gg O\left(\frac{c}{B}\right).$$

By compensation, we mean that once we estimated $\vec{\mathbf{m}}(s) \cdot \vec{\boldsymbol{\mu}}(s)$, we can replace in all the subsequent processing the ideal platform locations $\vec{\mathbf{r}}_p(s)$ by $\vec{\mathbf{r}}_p(s) + (\vec{\mathbf{m}}(s) \cdot \vec{\boldsymbol{\mu}}(s))\vec{\mathbf{m}}(s)$. We assume from now on that such a compensation has been made.

We now introduce some simple, conservative bounds on the norm of the trajectory perturbation $\vec{\boldsymbol{\mu}}(s)$ and its derivatives with respect to the slow time s. They are conservative in the sense that they are sufficient for the sensitivity analysis presented here and for the autofocus analysis presented in Section 4.

We assume in (3.19) that the norm of the trajectory perturbations is bounded by

$$|\vec{\boldsymbol{\mu}}(s)| \sim \overline{\mu} \ll \sqrt{\lambda_o L} \ll a, \tag{3.20}$$

with the second inequality being a consequence of the smallness of the inverse Fresnel number $\lambda_o L/a^2 \ll 1$ in (3.15). The speed $|\vec{\boldsymbol{\mu}}'(s)|$ should be a small fraction of V. We scale it using a dimensionless parameter δ, so that

$$S|\vec{\boldsymbol{\mu}}'(s)| \sim \frac{\lambda_o L}{a\delta} \ll a \quad \text{for} \quad S = a/(2V), \quad \delta \gg \frac{\lambda_o L}{a^2.} \quad \text{and} \quad \delta \gg \frac{\overline{\mu}}{a}. \tag{3.21}$$

This implies $|\vec{\boldsymbol{\mu}}'(s)| \ll V$, and it says that over the short time interval S defining the sub-aperture, the deviation of the platform from the unperturbed trajectory is much smaller than a, but it may be larger than the spot size $\lambda_o L/a$, depending on δ. The first assumption on δ implies, along with (3.6), that $\delta \gg B/\nu_o$ for target speeds $u \lesssim V$. We also take $\delta \gg \overline{\mu}/a$.

We assume next that the acceleration of the trajectory perturbation satisfies

$$S^2|\vec{\boldsymbol{\mu}}''(s)| \sim \frac{\lambda_o}{\gamma} \ll \frac{\lambda_o L}{a} \quad \text{for} \quad S = a/(2V), \tag{3.22}$$

where we have introduced another dimensionless parameter $\gamma \gg a/L$. Moreover,

$$S^3|\vec{\boldsymbol{\mu}}'''(s)| \ll \lambda_o \tag{3.23}$$

so that we can approximate $\vec{\boldsymbol{\mu}}(s+\tilde{s})$ by a second degree polynomial in $\tilde{s}$ over the small time interval $|\tilde{s}| \leq S$ used in the motion estimation,

$$\vec{\boldsymbol{\mu}}(s+\tilde{s}) \approx \vec{\boldsymbol{\mu}}(s) + \tilde{s}\vec{\boldsymbol{\mu}}'(s) + \frac{\tilde{s}^2}{2}\vec{\boldsymbol{\mu}}''(s). \tag{3.24}$$

It is convenient in the sensitivity analysis to assume that $\gamma \sim \delta$ so that we can work with the single dimensionless parameter $\varepsilon = \min\{1, \gamma, \delta\}$, which according to our assumptions above satisfies

$$\varepsilon \gg \frac{\lambda_o L}{a^2}\ , \quad \varepsilon \gg \frac{B}{\nu_o} \ \text{ and } \ \varepsilon \gg \frac{\overline{\mu}}{a}. \tag{3.25}$$

This allows us to linearize phases and express the Wigner transforms and the ambiguity functions in terms of sincs, rather than Fresnel integrals.

Remark 4. *Let us illustrate the assumptions made in this section in the GOTCHA regime described in Appendix A: Assumption (3.19) says that $|\vec{\boldsymbol{\mu}}(s)| \ll 17m$. At one degree aperture $a = 124m$, we have $\lambda_o L/a^2 = 0.02$, $B/\nu_o = 0.06$ and so we can choose in (3.25) $\varepsilon \gtrsim 0.3$. This gives in (3.21) $|\vec{\boldsymbol{\mu}}'|/V \lesssim 0.1$, that is $|\vec{\boldsymbol{\mu}}'| \lesssim 25km/h \approx 7m/s$ and in (3.22) $|\vec{\boldsymbol{\mu}}''| \lesssim 648km/h^2 = 0.05m/s^2$. These are very conservative bounds. In fact, when we look in detail at the calculations in Appendix D, we see that if we keep track of all the multiplicative constants, the results stated below would hold for accelerations that can be about twenty times larger than this. The same applies to the assumption (3.23) on $|\vec{\boldsymbol{\mu}}'''|$.*

3.4.2. ***Sensitivity of motion estimation to SAR platform trajectory perturbations.*** With the scaling above, we obtain the following results proved in Appendix D.

Proposition 4. *The Wigner transform of the range compressed data takes the form*

$$\mathcal{W}(s,\Omega,\omega_o,T) \sim \frac{|\widehat{f}_B(0)|^4}{|\vec{\mathbf{r}}_p(s)-\vec{\boldsymbol{\rho}}(s)|^4} sinc\left\{\pi B\left[T+\delta T^{\mathcal{W}}-\Delta\tau(s)\right]\right\} sinc\left\{\frac{4\pi a}{\lambda_o}\left[\frac{c(\Omega+\delta\Omega^{\mathcal{W}})}{2V\omega_o}-\Phi(s)\right]\right\}, \tag{3.26}$$

where $\sim$ denotes approximate, up to a multiplicative constant, $\Delta\tau(s)$ and $\Phi(s)$ are given in (3.4) and

$$\delta T^{\mathcal{W}} = \frac{2\vec{\boldsymbol{\mu}}(s)\cdot\vec{\mathbf{m}}(s)}{c}, \qquad \frac{c\delta\Omega^{\mathcal{W}}}{2V\omega_o} = \frac{\vec{\boldsymbol{\mu}}'(s)}{V}\cdot\vec{\mathbf{m}}(s) + \left(\vec{\mathbf{t}}(s) - \frac{\vec{\mathbf{u}}}{V}\right)\cdot\frac{\mathbb{P}(s)\vec{\boldsymbol{\mu}}(s)}{|\vec{\mathbf{r}}_p(s)-\vec{\boldsymbol{\rho}}(s)|}.$$

The ambiguity function evaluated at $\tilde{s} = a/(2V)$ has the form

$$\mathcal{A}\left(s,\Omega,\frac{a}{2V},T\right) \sim \frac{|\widehat{f}_B(0)|^4 e^{-\frac{i\omega_o a}{c}\left[\frac{c\,\delta T^{\mathcal{A}}}{a}+\Phi(s)\right]}}{|\vec{\mathbf{r}}_p(s)-\vec{\boldsymbol{\rho}}(s)|^4} sinc\left\{\frac{\pi B a}{c}\left[\frac{c(T+\delta T^{\mathcal{A}})}{a}+\Phi(s)\right]\right\} \times sinc\left[\frac{a(\Omega+\delta\Omega^{\mathcal{A}})}{2V}+\frac{\pi a^2\Phi^{\perp}(s)}{\lambda_o|\vec{\mathbf{r}}_p(s)-\vec{\boldsymbol{\rho}}(s)|}\right], \tag{3.27}$$

where $\Phi^{\perp}(s)$ is the same as in (3.12) and

$$\delta T^{\mathcal{A}} = -\frac{a}{V}\frac{\delta\Omega^{\mathcal{W}}}{\omega_o} \quad \text{and} \quad \frac{\delta\Omega^{\mathcal{A}}}{\omega_o} = \frac{Va}{c}\left[\frac{2\left(\vec{\mathbf{t}}-\frac{\vec{\mathbf{u}}}{V}\right)}{|\vec{\mathbf{r}}_p(s)-\vec{\boldsymbol{\rho}}(s)|}\cdot\frac{\mathbb{P}(s)\vec{\boldsymbol{\mu}}'(s)}{V}+\frac{\vec{\boldsymbol{\mu}}''(s)}{V^2}\cdot\vec{\mathbf{m}}(s)\right].$$

The results stated in this proposition are quite intuitive. When we combine the expressions of $\delta T^{\mathcal{W}}$ and $\delta\Omega^{\mathcal{W}}$ with those of $\Delta\tau(s)$ and $\Phi(s)$, given by (3.4), we see that equation (3.26) is the Wigner transform of the range compressed echo from a target located at $\vec{\boldsymbol{\rho}}(s) - \vec{\boldsymbol{\mu}}(s)$ at the instant corresponding to the center of the sub-aperture, and with velocity $\vec{\mathbf{u}} - \vec{\boldsymbol{\mu}}'(s)$. Similarly, (3.27) is the ambiguity function for target speed $\vec{\mathbf{u}} - \vec{\boldsymbol{\mu}}'(s)$ and acceleration $-\vec{\boldsymbol{\mu}}''(s)$. Since this is a relative motion between the target and the platform, it

is not confined to the imaging plane, in general. In any case, only projections of the relative velocity and acceleration determine the location of the peaks of the Wigner transform and ambiguity function of the data.

We conclude from Proposition 4 that the platform perturbations induce an error of the order $\vec{\boldsymbol{\mu}}(s)\cdot\vec{\mathbf{m}}(s)/c$ in the travel time estimation with the Wigner transform. As explained in the beginning of the previous section, this perturbation is within the main lobe of the first sinc function in $\mathcal{W}$, with resolution $O(1/B)$. It has therefore a small effect on the travel time estimation. However, the target motion estimation is affected by the platform trajectory perturbations. Explicitly, we have the errors

$$\frac{c\delta\Omega^{\mathcal{W}}}{V\omega_o} = O\left(\frac{|\vec{\boldsymbol{\mu}}'(s)\cdot\vec{\mathbf{m}}(s)|}{V} + \frac{|\vec{\boldsymbol{\mu}}(s)|}{L}\right) = O\left(\frac{\lambda_o L}{a^2\varepsilon} + \frac{\overline{\mu}}{L}\right) \tag{3.28}$$

in the estimation of $\vec{\mathbf{u}}/V\cdot\vec{\mathbf{m}}(s)$, and errors

$$\frac{c\delta\Omega^{\mathcal{A}}}{Va\omega_o} = O\left(\left|\mathbb{P}(s)\frac{\vec{\boldsymbol{\mu}}'(s)}{V}\right| + \frac{L|\vec{\boldsymbol{\mu}}''(s)\cdot\vec{\mathbf{m}}(s)|}{V^2}\right) \sim O\left(\frac{\lambda_o L}{a^2\varepsilon}\right) \tag{3.29}$$

in the estimation of $|\mathbb{P}(s)(\vec{\mathbf{t}}(s) - \vec{\mathbf{u}}/V)|^2$. Recalling from Section 3.2 that $\lambda_o L/a^2$ is the error bound on the estimated u/V with the unperturbed platform trajectory, we see that we can only approximate the target speed $\vec{\mathbf{u}}$ by $\vec{\mathbf{u}}^I$, with an error

$$\frac{|\Delta\vec{\mathbf{u}}|}{V} \lesssim \frac{\lambda_o L}{a^2\varepsilon}, \quad \text{where } \Delta\vec{\mathbf{u}} = \vec{\mathbf{u}}^{\mathcal{I}} - \vec{\mathbf{u}}\ , \tag{3.30}$$

and ε is defined by (3.25).

4. Autofocus with the Wigner transform and ambiguity function of the data.

As stated in Section 3.4, the SAR platform trajectory is known only approximately. The error in knowledge of the trajectory results in a shift and blur of the target image. The goal of the autofocus process described next is to estimate the phase errors, using the ambiguity function of data and its Wigner transform. Once we have estimated the phase errors, we can go back and use them in the image formation to get better resolution and to focus the image near the correct location. While Section 3.4 considered motion estimation in the more general situation of both target motion and platform perturbations, in this section we will approach the autofocus problem assuming that the target is stationary ($\vec{\mathbf{u}} = 0$), and located at $\vec{\boldsymbol{\rho}} = (\boldsymbol{\rho}, 0)$.

4.1. ***Effect of platform perturbations on image.***

Let us rewrite the imaging function (1.1) in terms of the range compressed data

$$\mathcal{I}(\boldsymbol{\rho}^{\mathcal{I}}) = \int_{-S}^{S} ds \int_{\omega_o-\pi B}^{\omega_o+\pi B} \frac{d\omega}{2\pi}\widehat{D}_r(s,\omega)e^{-\frac{2i\omega}{c}\left(|\vec{\mathbf{r}}_p(s)-\vec{\boldsymbol{\rho}}^{\,\mathcal{I}}|-|\vec{\mathbf{r}}_p(s)-\vec{\boldsymbol{\rho}}_o|\right)}, \tag{4.1}$$

where $\vec{\boldsymbol{\rho}}^{\,\mathcal{I}} = (\boldsymbol{\rho}^{\mathcal{I}}, 0)$ is the search point in the horizontal image plane. We take for convenience the origin of the slow time at the center of the aperture. We also let, for simplicity, the reference point $\vec{\boldsymbol{\rho}}_o$ in the data range compression be at the target. The data model is given by (2.11).

The focusing of the preliminary image $\mathcal{I}(\boldsymbol{\rho}^{\mathcal{I}})$ is described in Proposition 5. Its proof is similar to that of Proposition 4 and we do not include it here. It involves approximation of phases by a second degree polynomial in s, and careful justification of the approximations, using the scaling in Section 3.4.1, and the same constraints on the aperture as in Proposition 2.

Hereafter, we use the convention that when the arguments are missing, we evaluate the function at the slow time $s = 0$ indexing the center of the aperture. Explicitly, we let $\vec{\mathbf{r}}_p = \vec{\mathbf{r}}_p(0)$, $\vec{\mathbf{m}} = \vec{\mathbf{m}}(0) = \frac{\vec{\mathbf{r}}_p - \vec{\boldsymbol{\rho}}}{|\vec{\mathbf{r}}_p - \vec{\boldsymbol{\rho}}|}$, and so on.

Proposition 5. *The image $\mathcal{I}(\boldsymbol{\rho}^{\mathcal{I}})$ is given by*

$$\mathcal{I}(\boldsymbol{\rho}^{\mathcal{I}}) \sim \int_{\omega_o - \pi B}^{\omega_o + \pi B} d\omega \; exp\left\{ \frac{2i\omega}{c} \left(|\vec{\mathbf{r}}_p - \vec{\boldsymbol{\rho}}| - |\vec{\mathbf{r}}_p - \vec{\boldsymbol{\rho}}^{\,\mathcal{I}}| + \varphi_0 \right) \right\} \int_{-S}^{S} ds \; exp\left\{ \frac{2i\omega s V}{c} \left[\vec{\mathbf{t}} \cdot (\vec{\mathbf{m}} - \vec{\mathbf{m}}^{\mathcal{I}}) + \varphi_1 \right] + \frac{i\omega_o (sV)^2}{c} \left[\frac{\vec{\mathbf{t}}'}{V} \cdot (\vec{\mathbf{m}} - \vec{\mathbf{m}}^{\mathcal{I}}) + \frac{\left| \mathbb{P}\, \vec{\mathbf{t}} \right|^2}{|\vec{\mathbf{r}}_p - \vec{\boldsymbol{\rho}}|} - \frac{\left| \mathbb{P}^{\mathcal{I}} \vec{\mathbf{t}} \right|^2}{|\vec{\mathbf{r}}_p - \vec{\boldsymbol{\rho}}_\star^{\mathcal{I}}|} + \varphi_2 \right] \right\}, \tag{4.2}$$

where the symbol $\sim$ denotes approximate, up to a multiplicative constant. The focusing of $\mathcal{I}(\boldsymbol{\rho}^{\mathcal{I}})$ is determined by the phases

$$\varphi_o = \vec{\mathbf{m}} \cdot \vec{\boldsymbol{\mu}}, \tag{4.3}$$

$$\varphi_1 = \vec{\mathbf{m}} \cdot \frac{\vec{\boldsymbol{\mu}}'}{V} + \vec{\mathbf{t}} \cdot \frac{\mathbb{P}\vec{\boldsymbol{\mu}}}{|\vec{\mathbf{r}}_p - \vec{\boldsymbol{\rho}}|}, \tag{4.4}$$

$$\varphi_2 = \vec{\mathbf{m}} \cdot \frac{\vec{\boldsymbol{\mu}}''}{V^2} + \frac{2\left(\vec{\mathbf{t}} + \frac{\vec{\boldsymbol{\mu}}'}{V} \right)}{|\vec{\mathbf{r}}_p - \vec{\boldsymbol{\rho}}|} \cdot \frac{\mathbb{P}\vec{\boldsymbol{\mu}}'}{V}. \tag{4.5}$$

Here we denote by $\vec{\boldsymbol{\rho}}_\star^{\mathcal{I}} = (\boldsymbol{\rho}_\star^{\mathcal{I}}, 0)$ the image peak and we let $\vec{\mathbf{m}}^{\mathcal{I}} = \frac{\vec{\mathbf{r}}_p - \vec{\boldsymbol{\rho}}^{\,\mathcal{I}}}{|\vec{\mathbf{r}}_p - \vec{\boldsymbol{\rho}}^{\,\mathcal{I}}|}$, and $\mathbb{P}^{\mathcal{I}} = I - \vec{\mathbf{m}}^{\mathcal{I}} (\vec{\mathbf{m}}^{\mathcal{I}})^T$.

The Fresnel integral over s in (4.2) peaks when

$$\vec{\mathbf{t}} \cdot (\vec{\mathbf{m}} - \vec{\mathbf{m}}_\star^{\mathcal{I}}) = -\varphi_1, \qquad \vec{\mathbf{m}}_\star^{\mathcal{I}} = \frac{\vec{\mathbf{r}}_p - \vec{\boldsymbol{\rho}}_\star^{\mathcal{I}}}{|\vec{\mathbf{r}}_p - \vec{\boldsymbol{\rho}}_\star^{\mathcal{I}}|}, \tag{4.6}$$

and the integral over the bandwidth peaks when

$$|\vec{\mathbf{r}}_p - \vec{\boldsymbol{\rho}}| - |\vec{\mathbf{r}}_p - \vec{\boldsymbol{\rho}}_\star^{\mathcal{I}}| = -\varphi_0. \tag{4.7}$$

Linearizing about the true target location, we get that the peak $\vec{\boldsymbol{\rho}}_\star^{\mathcal{I}}$ of the image is shifted in range and cross-range by

$$\left| \vec{\mathbf{m}} \cdot (\vec{\boldsymbol{\rho}} - \vec{\boldsymbol{\rho}}_\star^{\mathcal{I}}) \right| = O(\varphi_0) \lesssim O\left(\frac{c}{B} \right), \qquad \left| \vec{\mathbf{t}} \cdot \frac{\mathbb{P}(\vec{\boldsymbol{\rho}} - \vec{\boldsymbol{\rho}}_\star^{\mathcal{I}})}{|\vec{\mathbf{r}}_p - \vec{\boldsymbol{\rho}}|} \right| = O(\varphi_1) \sim \frac{\lambda_o L}{a^2 \varepsilon}. \tag{4.8}$$

In the autofocus process we aim to estimate the phases $\varphi_o, \varphi_1, \varphi_2$, and then compensate the SAR platform trajectory perturbations to improve the image. The phases φ_0 and φ_1 affect the location of the peak of the image, as described in (4.8). The peak shift in range is small, within the resolution limits, but the shift in cross-range may be large. Because φ_2 appears in the quadratic part of the phase in (4.2), it only affects the spread of the image in cross-range, around its peak. The quadratic phase in (4.2) also depends on the shift $\vec{\boldsymbol{\rho}}_\star^{\mathcal{I}} - \vec{\boldsymbol{\rho}}$ of the peak of the image from the true target location. The larger the shift, the larger the phase and the more blur in the image.

We explain next how to estimate the phases φ_j, for $j = 0, 1, 2$, using the Wigner transform and ambiguity function. The autofocus process consists in applying the correction

$$\vec{\boldsymbol{\mu}}^{AF}(s) = \left[\varphi_o + sV\, \varphi_1 + \frac{(sV)^2}{2} \varphi_2 \right] \vec{\mathbf{m}}, \tag{4.9}$$

to the SAR platform trajectory

$$\vec{\mathbf{r}}_p(s) \rightsquigarrow \vec{\mathbf{r}}_p(s) + \vec{\boldsymbol{\mu}}^{AF}(s), \tag{4.10}$$

and forming the image

$$\mathcal{I}^{AF}(\boldsymbol{\rho}^{\mathcal{I}}) = \int_{-S}^{S} ds \int_{\omega_o - \pi B}^{\omega_o + \pi B} \frac{d\omega}{2\pi} \widehat{D}_r(s,\omega) e^{-\frac{2i\omega}{c}\left(|\vec{\mathbf{r}}_p(s) + \vec{\boldsymbol{\mu}}^{AF}(s) - \vec{\boldsymbol{\rho}}^{\mathcal{I}}| - |\vec{\mathbf{r}}_p(s) - \vec{\boldsymbol{\rho}}_o|\right)}. \tag{4.11}$$

We cannot estimate the trajectory perturbation

$$\vec{\boldsymbol{\mu}}(s) \approx \vec{\boldsymbol{\mu}} + s\vec{\boldsymbol{\mu}}' + \frac{s^2}{2}\vec{\boldsymbol{\mu}}''$$

from the three phases. It is is only the combination of the perturbation location, speed and acceleration that comes into play in (4.3-4.5) and affects the image. Thus, we compensate the effect of the trajectory perturbations with (4.9), as if we could neglect the second terms in (4.4-4.5).

4.2. ***Autofocus with the Wigner transform and ambiguity function.***

Setting $\vec{\mathbf{u}} = 0$ in Proposition 4, we obtain that the Wigner transform evaluated at $\omega = \omega_o$ takes the form

$$\mathcal{W}(s=0,\Omega,\omega_o,T) \sim \frac{|\widehat{f}_B(0)|^4}{|\vec{\mathbf{r}}_p - \vec{\boldsymbol{\rho}}|^4} \mathrm{sinc}\left\{\pi B\left[T + \delta T^{\mathcal{W}}\right]\right\} \mathrm{sinc}\left\{\frac{4\pi a c(\Omega + \delta\Omega^{\mathcal{W}})}{2\lambda_o V \omega_o}\right\}, \tag{4.12}$$

where

$$\delta T^{\mathcal{W}} = \frac{2\vec{\boldsymbol{\mu}} \cdot \vec{\mathbf{m}}}{c}, \qquad \frac{c\delta\Omega^{\mathcal{W}}}{2V\omega_o} = \vec{\mathbf{m}} \cdot \frac{\vec{\boldsymbol{\mu}}'}{V} + \vec{\mathbf{t}} \cdot \frac{\mathbb{P}\vec{\boldsymbol{\mu}}}{|\vec{\mathbf{r}}_p - \vec{\boldsymbol{\rho}}|}. \tag{4.13}$$

We evaluate the Wigner transform at $s = 0$, because that is the convention for the center of the sub-aperture assumed in this section. If we have overlapping sub-apertures, then the origin of the slow time s should be shifted for each aperture. Using (4.13) and (4.3-4.4), we have the following two estimates from the peaks $(\Omega^{\mathcal{W}}, T^{\mathcal{W}})$ of the Wigner transform, in the phase space (frequency-time plane) (Ω, T),

$$\varphi_o(s) = -\frac{c}{2}T^{\mathcal{W}}(s) + O\left(\frac{c}{B}\right), \qquad \varphi_1(s) = -\frac{\lambda_o}{4\pi V}\Omega^{\mathcal{W}}(s) + O\left(\frac{\lambda_o}{a}\right). \tag{4.14}$$

Proposition 4 also gives that the ambiguity function evaluated at $\tilde{s} = a/(2V)$ has the form

$$\mathcal{A}\left(s=0,\Omega,\frac{a}{2V},T\right) \sim \frac{|\widehat{f}_B(0)|^4 e^{-i\omega_o \delta T^{\mathcal{A}}}}{|\vec{\mathbf{r}}_p - \vec{\boldsymbol{\rho}}|^4} \mathrm{sinc}\left\{\pi B(T + \delta T^{\mathcal{A}})\right\} \mathrm{sinc}\left[\frac{a(\Omega + \delta\Omega^{\mathcal{A}})}{2V}\right], \tag{4.15}$$

where

$$\delta T^{\mathcal{A}} = -\frac{a}{V}\frac{\delta\Omega^{\mathcal{W}}}{\omega_o} \quad \text{and} \quad \frac{\delta\Omega^{\mathcal{A}}}{\omega_o} = \frac{Va}{c}\left[\frac{2\left(\vec{\mathbf{t}} - \frac{\vec{\mathbf{u}}}{V}\right)}{|\vec{\mathbf{r}}_p - \vec{\boldsymbol{\rho}}|} \cdot \frac{\mathbb{P}\vec{\boldsymbol{\mu}}'}{V} + \frac{\vec{\boldsymbol{\mu}}''}{V^2} \cdot \vec{\mathbf{m}}\right].$$

Using (4.4-4.5) and letting $(\Omega^{\mathcal{A}}, T^{\mathcal{A}})$ be the peaks of (4.15), we obtain that

$$\varphi_1(s) = \frac{c}{2a}T^{\mathcal{A}}(s) + O\left(\frac{c}{aB}\right), \qquad \varphi_2(s) = -\frac{\lambda_o}{2\pi aV}\Omega^{\mathcal{A}}(s) + O\left(\frac{\lambda_o}{a^2}\right). \tag{4.16}$$

Similar to what we have seen in the motion estimation problem in Section 3.2, we get a redundant estimate of φ_1, with worse resolution than that in (4.13), because

$$\frac{c}{aB} \sim \frac{\lambda_o}{a}\frac{\omega_o}{B} \gg \frac{\lambda_o}{a}.$$

The ambiguity function is useful for the estimation of φ_2, and thus complements the Wigner transform in the autofocus process.

As we remarked above, the Wigner transform and ambiguity function in (4.12) and (4.15) are for the sub-aperture centered at slow time $s = 0$. The autofocus process involves working with overlapping sub-apertures, with centers indexed by $\bar{s}$. Each sub-aperture gives an estimate of the three phases, $\varphi_j(\bar{s})$, for $j = 0, 1, 2$, and they can be combined to improve the compensation (4.9) of the platform trajectory perturbations. We illustrate this in Section 6, where we present numerical results.

5. Autofocus with centroids of the Wigner transform and ambiguity function

The peak selection used in the previous section for the autofocus process may be problematic in practice, specially in noisy environments. It is also computationally expensive because accurate peak selection requires a very fine sampling of the phase space (frequency-time plane) in which we evaluate the Wigner transform and ambiguity function. We show in Section 5.2 that the centroids of the Wigner transform and ambiguity function of data from an imaging scene with a strong target give in theory exactly the same information as the peaks. Thus, we can do the autofocus with the centroids, which are more robust than the peak selection, because they are given by smooth functionals (integrals) of the Wigner transform and ambiguity function.

When there are multiple strong targets at locations $\vec{\boldsymbol{\rho}}_k$ and similar range from the SAR platform, we cannot separate their pulse compressed echoes by time windowing, as we have assumed in the previous section. Then, the Wigner transform and ambiguity function have multiple peaks in the phase space, even when we neglect multiple scattering between the targets and write the data model as

$$\widehat{D}_r(s,\omega) \approx \sum_{k=1}^{N} \frac{\omega_o^2}{c^2} \frac{\left|\widehat{f}_B(0)\right|^2 e^{i\omega_o \psi(0)}}{(4\pi|\vec{\mathbf{r}}_p(s) - \vec{\boldsymbol{\rho}}_k|)^2} e^{\frac{2i\omega}{c}(|\vec{\mathbf{r}}_p(s)+\vec{\boldsymbol{\mu}}(s)-\vec{\boldsymbol{\rho}}_k|-|\vec{\mathbf{r}}_p(s)-\vec{\boldsymbol{\rho}}_o|)}. \tag{5.1}$$

Roughly speaking, there is one peak per target at locations similar to those described in Section 4.2, for $\vec{\boldsymbol{\rho}} \rightsquigarrow \vec{\boldsymbol{\rho}}_k$ and $k = 1, 2, \ldots, N$. There are also additional peaks coming from the cross-terms $k \neq k'$ in the quadratic expressions of the Wigner transforms and ambiguity functions. It is not clear in such cases how to select a particular peak in the phase space in order to carry out the autofocus process, but we may be able to use the centroids. We show in Section 5.3 that the centroids are useful for estimating the platform trajectory perturbations in the case of multiple targets that are not too spread out in the imaging plane. We also illustrate the performance of the autofocus process with numerical simulations in Section 6.

5.1. ***Definition.***

The centroid of the Wigner transform is the point $\left(\overline{\Omega^{\mathcal{W}}}(s), \overline{T^{\mathcal{W}}}(s)\right)$ in the phase space with coordinates

$$\begin{aligned}
\overline{\Omega^{\mathcal{W}}}(s) &= \frac{\int_{-\infty}^{\infty} d\Omega \int_{-\infty}^{\infty} dT\ \Omega\ \mathcal{W}(s,\Omega,\omega_o,T)}{\int_{-\infty}^{\infty} d\Omega \int_{-\infty}^{\infty} dT\ \mathcal{W}(s,\Omega,\omega_o,T)}, \\
\overline{T^{\mathcal{W}}}(s) &= \frac{\int_{-\infty}^{\infty} d\Omega \int_{-\infty}^{\infty} dT\ T\ \mathcal{W}(s,\Omega,\omega_o,T)}{\int_{-\infty}^{\infty} d\Omega \int_{-\infty}^{\infty} dT\ \mathcal{W}(s,\Omega,\omega_o,T)}.
\end{aligned} \tag{5.2}$$

With our notation convention, the aperture is centered at $s = 0$, and we let $\overline{\Omega^{\mathcal{W}}} = \overline{\Omega^{\mathcal{W}}}(0)$ and $\overline{T^{\mathcal{W}}} = \overline{T^{\mathcal{W}}}(0)$. The centroid $\left(\overline{\Omega^{\mathcal{A}}}, \overline{T^{\mathcal{A}}}\right)$ of the ambiguity function $\mathcal{A}\left(s = 0, \Omega, \frac{a}{2V}, \Omega\right)$ is defined similarly.

To relate the centroids to the phases that arise in the autofocus process, we need the following result, which we state for an arbitrary center s of the aperture, not just $s = 0$:

Lemma 1. *The centroid of the Wigner transform of the range compressed data has the form*

$$\overline{\Omega^{\mathcal{W}}}(s) = \frac{i\left[\frac{\partial}{\partial s}\widehat{D}_r\left(s,\omega_o\right)\overline{\widehat{D}_r\left(s,\omega_o\right)} - \widehat{D}_r\left(s,\omega_o\right)\overline{\frac{\partial}{\partial s}\widehat{D}_r\left(s,\omega_o\right)}\right]}{2|\widehat{D}_r\left(s,\omega_o\right)|^2},$$

$$\overline{T^{\mathcal{W}}}(s) = -\frac{i\left[\frac{\partial}{\partial \omega}\widehat{D}_r\left(s,\omega\right)\overline{\widehat{D}_r\left(s,\omega_o\right)} - \widehat{D}_r\left(s,\omega_o\right)\overline{\frac{\partial}{\partial \omega}\widehat{D}_r\left(s,\omega_o\right)}\right]}{2|\widehat{D}_r\left(s,\omega_o\right)|^2}.$$

Similarly, the centroid of the ambiguity function satisfies, for $\tilde{s} = a/(2V)$,

$$\overline{\Omega^{\mathcal{A}}}(s) = \frac{i\left[\frac{\partial}{\partial s}\widehat{D}_r\left(s+\frac{\tilde{s}}{2},\omega_o\right)\overline{\widehat{D}_r\left(s-\frac{\tilde{s}}{2},\omega_o\right)} + \widehat{D}_r\left(s+\frac{\tilde{s}}{2},\omega_o\right)\overline{\frac{\partial}{\partial s}\widehat{D}_r\left(s-\frac{\tilde{s}}{2},\omega_o\right)}\right]}{\widehat{D}_r\left(s+\frac{\tilde{s}}{2},\omega_o\right)\overline{\widehat{D}_r\left(s-\frac{\tilde{s}}{2},\omega_o\right)}},$$

$$\overline{T^{\mathcal{A}}}(s) = -\frac{i\left[\frac{\partial}{\partial \omega}\widehat{D}_r\left(s+\frac{\tilde{s}}{2},\omega_o\right)\overline{\widehat{D}_r\left(s-\frac{\tilde{s}}{2},\omega_o\right)} + \widehat{D}_r\left(s+\frac{\tilde{s}}{2},\omega_o\right)\overline{\frac{\partial}{\partial \omega}\widehat{D}_r\left(s-\frac{\tilde{s}}{2},\omega_o\right)}\right]}{\widehat{D}_r\left(s+\frac{\tilde{s}}{2},\omega_o\right)\overline{\widehat{D}_r\left(s-\frac{\tilde{s}}{2},\omega_o\right)}}.$$

These expressions follow from the definition (5.2) of the centroids and definitions (3.1) and (3.10) of the Wigner transform and ambiguity function. Explicitly, we have from (3.1) that

$$\begin{aligned}\int_{-\infty}^{\infty} d\Omega \int_{-\infty}^{\infty} dT\, \mathcal{W}(s,\Omega,\omega_o,T) &= 4\pi^2 \int_{-\tilde{\Omega}}^{\tilde{\Omega}} d\tilde{\omega} \int_{-\tilde{S}}^{\tilde{S}} d\tilde{s}\, \widehat{D}_r\left(s+\frac{\tilde{s}}{2},\omega_o+\frac{\tilde{\omega}}{2}\right)\overline{\widehat{D}_r\left(s-\frac{\tilde{s}}{2},\omega_o-\frac{\tilde{\omega}}{2}\right)} \\ &\qquad \int_{-\infty}^{\infty}\frac{d\Omega}{2\pi}e^{i\tilde{s}\Omega}\int_{-\infty}^{\infty}\frac{dT}{2\pi}e^{-i\tilde{\omega}T} \\ &= 4\pi^2\left(F_{s,\omega_o}(\tilde{s},\tilde{\omega}),\delta(\tilde{s},\tilde{\omega})\right).\end{aligned}$$

Here $\delta(\tilde{s},\tilde{\omega}) = \delta(\tilde{s})\delta(\tilde{\omega})$ is the Dirac delta distribution, acting on the test function $F_{s,\omega_o}(\tilde{s},\tilde{\omega})$ of arguments $\tilde{s},\tilde{\omega}$, and parametrized by s and ω_o. The test function is given by

$$F_{s,\omega_o}(\tilde{s},\tilde{\omega}) = \chi(\tilde{s},\tilde{\omega})\widehat{D}_r\left(s+\frac{\tilde{s}}{2},\omega_o+\frac{\tilde{\omega}}{2}\right)\overline{\widehat{D}_r\left(s-\frac{\tilde{s}}{2},\omega_o-\frac{\tilde{\omega}}{2}\right)},$$

with $\chi(\tilde{s},\tilde{\omega})$ an arbitrary, smooth window function with support in $[-\tilde{S},\tilde{S}]\times[-\tilde{\Omega},\tilde{\Omega}]$, that is equal to one in the vicinity of the origin. Similarly,

$$\begin{aligned}\int_{-\infty}^{\infty} d\Omega \int_{-\infty}^{\infty} dT\, \Omega\, \mathcal{W}(s,\Omega,\omega_o,T) &= 4\pi^2 \int_{-\tilde{\Omega}}^{\tilde{\Omega}} d\tilde{\omega} \int_{-\tilde{S}}^{\tilde{S}} d\tilde{s}\, \widehat{D}_r\left(s+\frac{\tilde{s}}{2},\omega_o+\frac{\tilde{\omega}}{2}\right)\overline{\widehat{D}_r\left(s-\frac{\tilde{s}}{2},\omega_o-\frac{\tilde{\omega}}{2}\right)} \\ &\qquad \int_{-\infty}^{\infty}\frac{d\Omega}{2\pi}\,\Omega\, e^{i\tilde{s}\Omega}\int_{-\infty}^{\infty}\frac{dT}{2\pi}e^{-i\tilde{\omega}T} \\ &= -4i\pi^2\left(F_{s,\omega_o}(\tilde{s},\tilde{\omega}),\delta_{\tilde{s}}(\tilde{s},\tilde{\omega})\right),\end{aligned}$$

where $\delta_{\tilde{s}}(\tilde{s},\tilde{\omega}) = \delta'(\tilde{s})\delta(\tilde{\omega})$. Thus, we have from the properties of the Dirac delta distribution that

$$\overline{\Omega^{\mathcal{W}}} = \frac{i\partial_{\tilde{s}}F_{s,\omega_o}(0,0)}{F_{s,\omega_o}(0,0)},$$

and its expression given in Lemma 1 follows. The proof of the expressions of $\overline{T^{\mathcal{W}}}$, $\overline{\Omega^{\mathcal{A}}}$ and $\overline{T^{\mathcal{A}}}$ is similar.

5.2. ***The case of a single target.***

Lemma 1 and the model (2.11) of the range compressed data give that

$$\overline{\Omega^{\mathcal{W}}} = \frac{2\omega_o V}{c}\Phi(s) - \delta\Omega^{\mathcal{W}}, \qquad \overline{T^{\mathcal{W}}} = \Delta\tau(s) - \delta T^{\mathcal{W}}, \tag{5.3}$$

where Φ and $\Delta\tau$ are given by (3.4) and $\delta\Omega^{\mathcal{W}}$ and $\delta T^{\mathcal{W}}$ are defined in Proposition 4. The centroid of the ambiguity function satisfies

$$\begin{aligned}
\overline{\Omega^{\mathcal{A}}}(s) =& -\frac{2\pi V a \Phi^{\perp}(s)}{\lambda_o |\vec{\mathbf{r}}_p(s) - \vec{\boldsymbol{\rho}}(s)|} - \delta\Omega^{\mathcal{A}} + O\left(\frac{Va^2}{\lambda_o L^2}\right), \\
\overline{T^{\mathcal{A}}}(s) =& -\frac{a}{c}\Phi(s) - \delta T^{\mathcal{A}} + O\left(\frac{a^3}{cL^2}\right),
\end{aligned} \tag{5.4}$$

where $\Phi^{\perp}$ is given in (3.12) and $\delta\Omega^{\mathcal{A}}$ and $\delta T^{\mathcal{A}}$ are defined in Proposition 4. These equations follow from Lemma 1 and the mean value theorem. The residuals come from estimates of the second derivatives of the range compressed data model, for slow time offsets that do not exceed $\tilde{s} = a/(2V)$.

When we discussed the autofocus in Section 4, we assumed a stationary target and took for simplicity the reference point $\vec{\boldsymbol{\rho}}_o$ in the range compression exactly at the target location $\vec{\boldsymbol{\rho}}$. Then, the phases Φ and $\Phi^{\perp}$ vanish and we note that the centroids coincide with the peaks of the Wigner transform and ambiguity function given in Section 4.2. Naturally, the equality of the centroids and the location of the peaks does hold for a moving target and for $\vec{\boldsymbol{\rho}}_o \neq \vec{\boldsymbol{\rho}}$, as follows from a straightforward calculation. The conclusion is that we can apply the results in the previous section, with the peaks replaced by the centroids, to do the autofocus of imaging scenes with a strong target.

5.3. ***Autofocus with Multiple Stationary Targets.***

We study here the centroids of the Wigner transform and ambiguity function in the case of N stationary targets. They are at similar ranges from the SAR platform, and thus their echoes cannot be separated by time windowing. The data model is given by (5.1), and it neglects multiple scattering between the targets. The assumption is that either the multiply scattered signals are weak, or that they arrive at a later time and may be filtered out by time windowing.

To study the centroids, we obtain from the data model that

$$\begin{aligned}
\frac{\partial}{\partial s}\widehat{D}_r(s,\omega_o) =& \sum_{k=1}^{N} \frac{2i\omega_o}{c}\left[V\vec{\mathbf{t}}(s)\cdot(\vec{\mathbf{m}}_k(s) - \vec{\mathbf{m}}_o(s)) + \vec{\boldsymbol{\mu}}'(s)\cdot\vec{\mathbf{m}}_k(s)\right]\widehat{D}_r^k(s,\omega_o), \\
\frac{\partial}{\partial\omega}\widehat{D}_r(s,\omega_o) =& \sum_{k=1}^{N} \frac{2i}{c}\left(|\vec{\mathbf{r}}_p(s) + \vec{\boldsymbol{\mu}}(s) - \vec{\boldsymbol{\rho}}_k| - |\vec{\mathbf{r}}_p(s) - \vec{\boldsymbol{\rho}}_o|\right)\widehat{D}_r^k(s,\omega_o),
\end{aligned}$$

where $\widehat{D}^k(s,\omega_o)$ is the Fourier transform of the range compressed echo from the $k-$th target at location $\vec{\boldsymbol{\rho}}_k$, and $\vec{\mathbf{m}}_k(s)$ is the unit vector pointing form the platform at $\vec{\mathbf{r}}_p(s)$ to $\vec{\boldsymbol{\rho}}_k$. The results below are derived from this equation and Lemma 1 by expanding around the reference point $\vec{\boldsymbol{\rho}}_o$.

We obtain that the centroid of the Wigner transform satisfies

$$\overline{\Omega^{\mathcal{W}}}(s) = \overline{\Omega_o^{\mathcal{W}}}(s) + \frac{\omega_o V}{c}\mathcal{E}_1, \qquad \overline{T^{\mathcal{W}}}(s) = \overline{T_o^{\mathcal{W}}}(s) + \frac{1}{B}\mathcal{E}_2, \tag{5.1}$$

where $\left(\overline{\Omega_o^{\mathcal{W}}}, \overline{T_o^{\mathcal{W}}}\right)$ is the centroid of the Wigner transform for a single target at $\vec{\boldsymbol{\rho}}_o$, and the dimensionless

residuals are given by

$$\mathcal{E}_1 = -\sum_{k,k'=1}^{N} (\vec{\boldsymbol{\rho}}_k + \vec{\boldsymbol{\rho}}_{k'} - 2\vec{\boldsymbol{\rho}}_o) \cdot \frac{\mathbb{P}(s)\left[\vec{\mathbf{t}}(s) + \vec{\boldsymbol{\mu}}'(s)/V\right]}{|\vec{\mathbf{r}}_p(s) - \vec{\boldsymbol{\rho}}_o|} \frac{\widehat{D}_r^k(s,\omega_o)\overline{D_r^{k'}(s,\omega_o)}}{|\widehat{D}_r(s,\omega_o)|^2},$$

and

$$\mathcal{E}_2 = \frac{B}{c}\sum_{k,k'=1}^{N} (\vec{\boldsymbol{\rho}}_k + \vec{\boldsymbol{\rho}}_{k'} - 2\vec{\boldsymbol{\rho}}_o) \cdot \vec{\mathbf{m}}_o(s) \frac{\widehat{D}_r^k(s,\omega_o)\overline{D_r^{k'}(s,\omega_o)}}{|\widehat{D}_r(s,\omega_o)|^2}.$$

Let us denote by $|\Delta\vec{\boldsymbol{\rho}}|$ the typical distance of a target from $\vec{\boldsymbol{\rho}}_o$, and by $|\Delta\vec{\boldsymbol{\rho}} \cdot \vec{\mathbf{m}}_o|$ the typical distance along the range direction $\vec{\mathbf{m}}_o$. The estimates of the residuals are

$$|\mathcal{E}_1| \lesssim O\left(\frac{|\Delta\vec{\boldsymbol{\rho}}|}{L}\right), \qquad |\mathcal{E}_2| \lesssim O\left(\frac{|\Delta\vec{\boldsymbol{\rho}} \cdot \vec{\mathbf{m}}_o|}{c/B}\right). \tag{5.2}$$

Similarly, we can estimate the centroid of the ambiguity function. We only need the result for $\overline{\Omega^{\mathcal{A}}(s)}$, because $\overline{T^{\mathcal{A}}(s)}$ gives basically the same information as $\overline{T^{\mathcal{W}}(s)}$, at worse resolution. We get

$$\overline{\Omega^{\mathcal{A}}(s)} = \overline{\Omega_o^{\mathcal{A}}(s)} + \frac{\omega_o V}{c}\mathcal{E}_3, \qquad |\mathcal{E}_3| \lesssim O\left(\frac{|\Delta\vec{\boldsymbol{\rho}}|}{L}\right), \tag{5.3}$$

where $\overline{\Omega_o^{\mathcal{A}}(s)}$ is the frequency coordinate of the centroid of the ambiguity function for a target at $\vec{\boldsymbol{\rho}}_o$.

We conclude that when the targets are not too spread out in the imaging plane, the centroids are approximately as those for a single target at $\vec{\boldsymbol{\rho}}_o$. Explicitly, if we have

$$\frac{|\Delta\vec{\boldsymbol{\rho}}|}{L} \ll \frac{|\vec{\boldsymbol{\mu}}' \cdot \vec{\mathbf{m}}_o|}{V}, \tag{5.4}$$

we can estimate $\vec{\boldsymbol{\mu}}' \cdot \vec{\mathbf{m}}_o$ from $\overline{\Omega^{\mathcal{W}}} \approx \overline{\Omega_o^{\mathcal{W}}}$. When we compensate this term in the image formation, we correct the shift in cross-range. If in addition

$$\frac{|\Delta\vec{\boldsymbol{\rho}}|}{L} \ll \frac{L|\vec{\boldsymbol{\mu}}'' \cdot \vec{\mathbf{m}}_o|}{V^2}, \tag{5.5}$$

we can estimate $\vec{\boldsymbol{\mu}}'' \cdot \vec{\mathbf{m}}_o$ from $\overline{\Omega^{\mathcal{A}}} \approx \overline{\Omega_o^{\mathcal{A}}}$, and then use the estimate to reduce the blur in the image. When we recall the assumptions in Section 3.4.1 on $\vec{\boldsymbol{\mu}}'$ and $\vec{\boldsymbol{\mu}}''$, we see that basically, the bounds in (5.4-5.5) say that the targets should be contained in a disk in the imaging plane of radius smaller than L, the range.

The second equations in (5.1) and (5.2) say that to determine the perturbation $\vec{\boldsymbol{\mu}} \cdot \vec{\mathbf{m}}_o$ from $\overline{T^{\mathcal{W}}}$, the projection of $\Delta\vec{\boldsymbol{\rho}}$ in the range direction $\vec{\mathbf{m}}_o$ must not exceed the range resolution c/B,

$$|\Delta\vec{\boldsymbol{\rho}} \cdot \vec{\mathbf{m}}_o| \ll \frac{c}{B}. \tag{5.6}$$

This condition may appear stringent, but if there were a larger range spread, we could separate the targets by simply time windowing the pulse compressed echoes.

Let us end this section with the remark that the results presented here extend naturally to the case of multiple targets that move the same way, as a group, with speed $\vec{\mathbf{u}}$. Then, it is the relative motion of the targets with respect to that of the SAR platform that is determined by the centroids of the Wigner transform and ambiguity function.

6. Numerical simulations.

We present in Section 6.1 results for target motion and no platform perturbations and in Section 6.2 results for autofocus. The data is generated with models (2.11), (5.1), with parameters chosen as in the GOTCHA Volumentric SAR regime described in Appendix A. The unperturbed SAR platform trajectory is circular, at altitude H, and with center projected at the origin $(0,0)$ in the imaging plane.

To compute the Wigner transform $\mathcal{W}$ and ambiguity function $\mathcal{A}$ for each s in a small a small aperture a, we need the range compressed data over a larger aperture $a_e = 2.5a$. We use the two-dimensional fast Fourier transform (FFT) to compute $\mathcal{W}$ and $\mathcal{A}$. To avoid aliasing, we pad with zeroes the $N_s \times N_\omega$ matrix with entries

$$\mathbb{D}_{s,\omega}(\tilde{s},\tilde{\omega}) = \widehat{D}_r\left(s+\frac{\tilde{s}}{2},\omega+\frac{\tilde{\omega}}{2}\right)\overline{\widehat{D}_r\left(s-\frac{\tilde{s}}{2},\omega-\frac{\tilde{\omega}}{2}\right)}.$$

Here s and ω are parameters, and $N_s = 118$ and $N_\omega = 424$ are the number of samples in $\tilde{s}$ and $\tilde{\omega}$. The padding creates a larger matrix, of size 256×1024, for each s in the slow time range and ω in the bandwidth. The motion estimation and autofocus is carried out either by selecting the peaks of the Wigner transform and ambiguity function, or by computing their centroids.

The preliminary images can be computed directly from (1.1), and the autofocused ones from (4.11). However, because of the small sub-apertures, we can compute them more efficiently by linearizing the phases and using the two dimensional FFT of the range compressed data.

6.1. ***Motion estimation without platform perturbations.***

We consider here a target moving with constant velocity $\mathbf{u} = 28/\sqrt{2}(1,1)$m/s. The aperture is $a = \pi R/180 \approx$ 124m. It corresponds to a one degree arc on the circular trajectory of radius $R = 7.1$km.

We show in Figure 2 the Wigner transform and ambiguity function evaluated at $s = 0$. Note the large spread of $\mathcal{A}$ in the time variable T. This is consistent with the resolution results in Section 3.2. We obtained there that the target speed projected in the range direction can be determined either form the peak $\Omega^{\mathcal{W}}$ of the Wigner transform or the peak $T^{\mathcal{A}}$ of the ambiguity function, but the resolution of the Wigner estimate is better. This is illustrated in Figure 2 by the tighter peak of the Wigner transform.

We estimate the target speed $\mathbf{u} \rightsquigarrow \mathbf{U}(s)$ using equations (3.7) and (3.14). We move the target from one center s of a sub-aperture to another $s \pm \Delta s$, with the estimated $\mathbf{U}(s)$. We plot in Figures 3 and 4 the actual and estimated projections of the velocity as in equations (3.7), (3.13) and (3.14). The estimates are shown in solid lines. The dotted lines indicate the resolution limits.

Because we assume that over a single aperture the target has a constant velocity, we average the multiple estimates $\mathbf{U}(s)$, from the overlapping sub-apertures, to get $\mathbf{u}^{\mathcal{I}}$. We use this estimated target speed to compute an image using equation (4.1), with $\vec{\boldsymbol{\rho}}^{\,\mathcal{I}} \rightsquigarrow \vec{\boldsymbol{\rho}}^{\,\mathcal{I}} + s(\mathbf{u}^{\mathcal{I}},0)$. The pixels are squares of side 0.1 m, and the image domain is 10m $\times$10m. The image is compared in Figure 6 with that computed with the exact target velocity. We also show in Figure 7 the error between the true target trajectory and the estimated one.

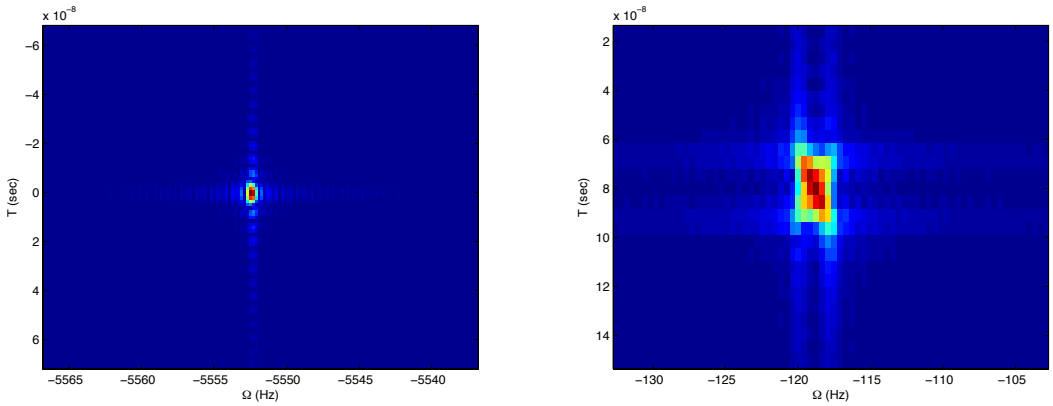

(a) Wigner transform $W(\Omega, T)$ (b) Ambiguity function $A(\Omega, T)$

Figure 2. The Wigner transform and Ambiguity function of the range compressed echoes from a single target.

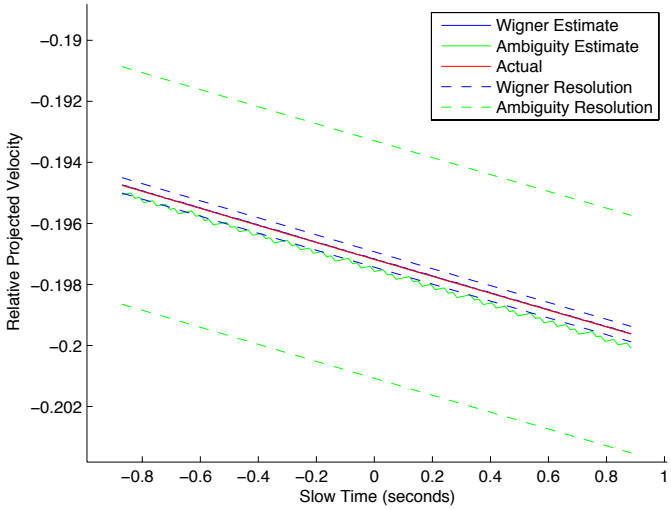

Figure 3. Estimated velocity projected onto $\vec{\mathbf{m}}(s)$. The Wigner estimate is in solid blue and the ambiguity one in solid green. The tue value is in solid red. The blue dotted line indicates the theoretical resolution limit for the Wigner estimates. The green dotted line shows the resolution limit for the estimates with the ambiguity function.

6.2. ***Autofocus with stationary targets.***

We begin with the case of a single stationary target at known location $\vec{\boldsymbol{\rho}} = (\boldsymbol{\rho}, 0)$. We take $\boldsymbol{\rho}$ at the origin and use the simple SAR platform trajectory perturbation

$$\vec{\boldsymbol{\mu}}(s) = \left(5\lambda_0 s + \frac{\lambda_0}{2}\frac{s^2}{2} + \frac{\lambda_0}{20}\frac{s^3}{6}, 30\lambda_0, 2\lambda_0 s - \frac{\lambda_0}{2}\frac{s^2}{2} + \frac{\lambda_0}{20}\frac{s^3}{6}\right),$$

that satisfies our assumptions in Section 3.4.1. The autofocus is done as described in Section 4, except that we use the centroids of the Wigner transform and ambiguity function to estimate the platform trajectory perturbation (4.9). The image before the autofocus is shown on the left in Figure 8. The peak is shifted

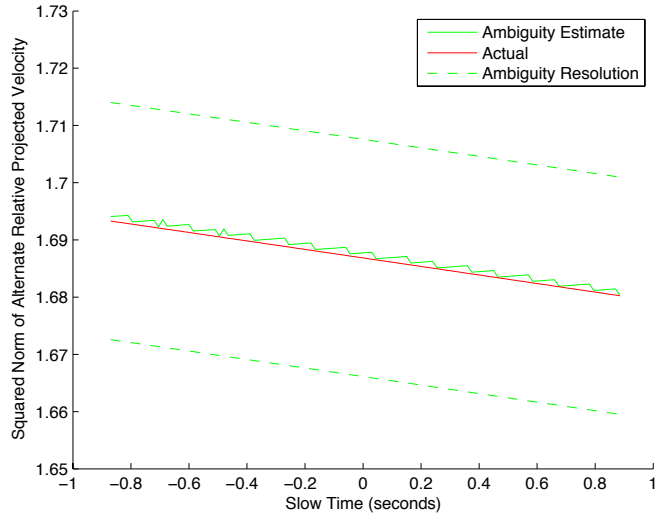

Figure 4. The estimated projected velocity in the direction orthogonal to $\vec{\mathbf{m}}(s)$, using the ambiguity function. The true value is in solid red and the estimate in solid green. The dotted green line indicates the resolution limits.

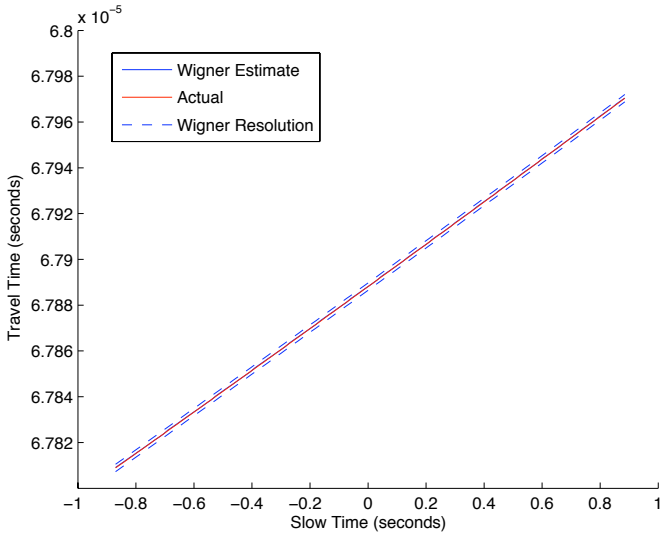

Figure 5. The estimated travel time using the Wigner transform. The true value is in red and the estimate is in solid blue. The dotted blue line denotes the resolution limits.

by 10m in cross-range from the target location. The autofocused image is shown on the right in Figure 8. It peaks near the target location, indicated with the black dot. It is also better focused in cross-range. The improved resolution can be seen in Figure 9, where we plot cross-sections of the image in range and cross-range. As expected from the theory, the range resolution is not affected by the SAR platform trajectory perturbation. It is the focusing in cross-range that is improved significantly by the autofocus process.

Let us consider now a scene with 81 stationary scatterers, and a sinusoidal trajectory perturbation that is more difficult to estimate. We show the perturbation along the range direction with the black solid line

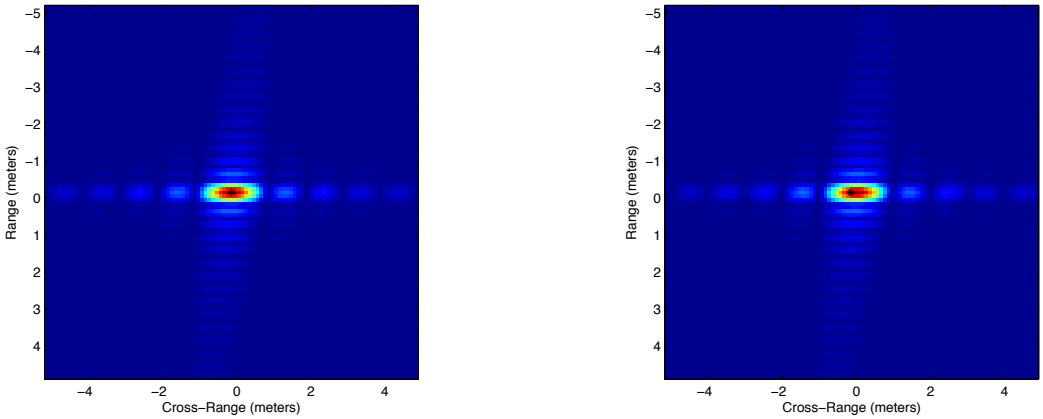

(a) Image with exact motion compensation

(b) Image compensated with motion estimation

Figure 6. Images of moving target computed with the true and estimated velocity.

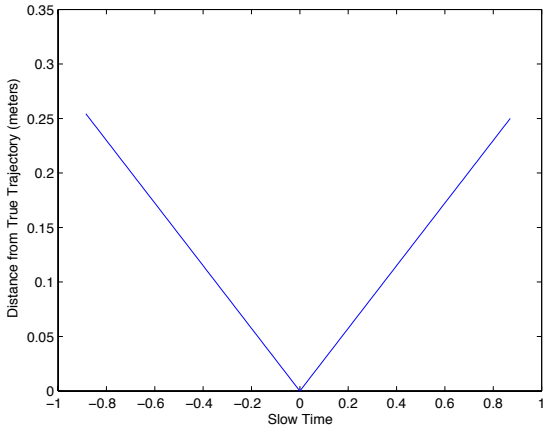

Figure 7. Error in meters between the true trajectory of the moving target and the trajectory estimated from the data over a single small aperture.

in the top left plot in Figure 11, and the imaging scene in the bottom left plot. The estimated trajectory perturbation is shown in blue in the top left picture. It is shifted from the true value, but this shift only affects the range focusing within the resolution limit c/B, and it has little effect on the image. The Wigner transform and ambiguity function are shown in Figure 10. The centroid is indicated with a black star. The images before and after autofocus are on the top and bottom right in Figure 11. These images are computed over an aperture of 1km, using the estimates from ten overlapping sub-apertures of 124m.

Figure 12 displays the results from another complex scene, created from a low-resolution aerial picture of a Stanford flower garden. Each pixel is treated as a point scatterer with reflectivity equal to its pixel value and the data is generated with the Born approximation. The aperture is as above, of 1km, consisting of ten overlapping sub-apertures of 124m. The platform trajectory perturbation is less oscillatory here, as shown with the black solid line in the top left plot. The estimated perturbation is shown in blue. The perfect image is in the bottom left plot, and the unfocussed and autofocused images are in the top right and bottom right

plots, respectively. The perfect image is for no SAR platform trajectory perturbations.

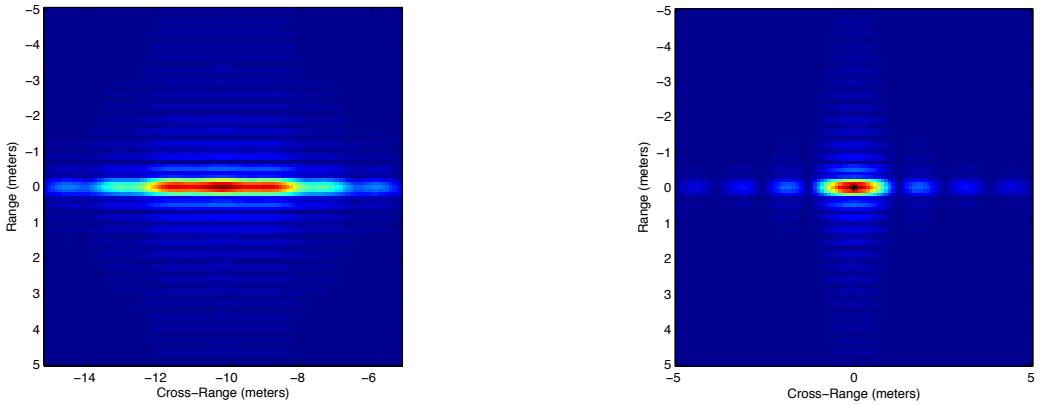

(a) Unfocused Image

(b) Autofocused Image

Figure 8. Images of a stationary target before and after autofocus. The image windows are the same size but the left one is translated to be center at the peak of the unfocused image, which is not at the target location. The autofocused image is on the right, and the tagret is indicated with a black dot.

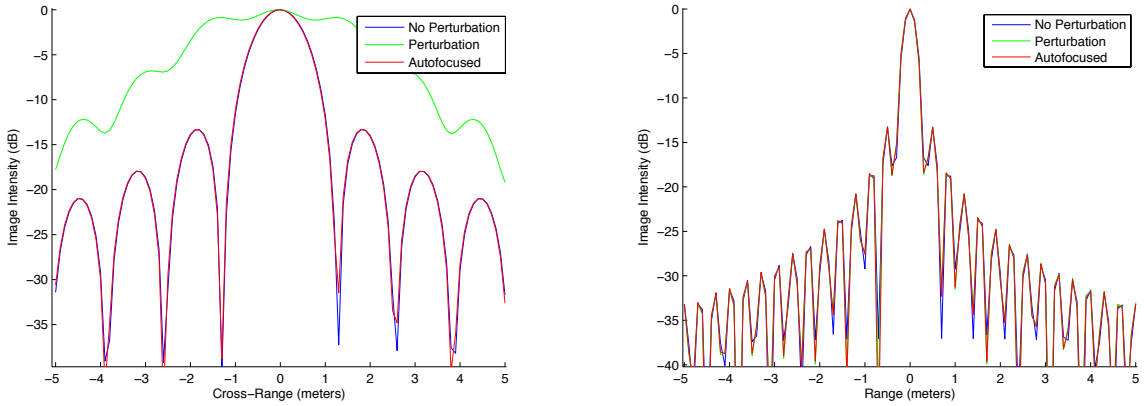

(a) Cross-range resolution

(b) Range Resolution

Figure 9. Cross-range and range resolution of images before and after autofocus. The platform perturbations affect only the cross-range focus. The autofocus improves the cross-range resolution and gives an image that is essentially identical to the ideal one, without any platform perturbations.

7. Summary and conclusions.

We have introduced and analyzed in detail from first principles a synthetic aperture radar (SAR) imaging and target motion estimation approach that is combined with compensation for radar platform trajectory perturbations. We have formulated an approach that implements the theory for a single target and a single small aperture and extends it to autofocus for scenes with multiple scatterers. This approach can deal with either target motion estimation or with SAR platform trajectory perturbation, but not with both. Combined estimation requires multi-target scenes and multiple, overlapping apertures where the basic

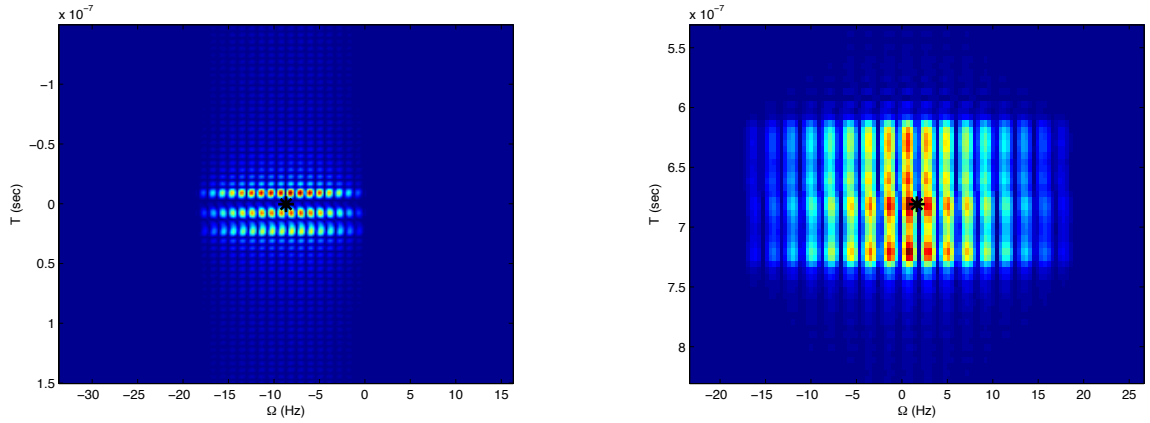

(a) Wigner transform $W(\Omega, T)$

(b) Ambiguity function $A(\Omega, T)$

Figure 10. The Wigner transform and ambiguity function of the range compressed echoes from an 81 stationary scatterer scene. The asterisk indicates the location of the centroid.

algorithm presented here is used as a component in a broader estimation and imaging strategy. In addition to providing detailed analytical error estimates for the approximations that we use, we verify that they are appropriate for the regime that arises in the GOTCHA Volumetric SAR data set. We also assess the performance of this approach with detailed numerical simulations, presented in Section 6.

Acknowledgement

The work of L. Borcea was partially supported by the National Science Foundation, grants DMS-0604008, DMS-0934594, DMS-0907746, by the Office of Naval Research grants N000140910290 and N000140510699, and by Air Force - SBIR FA8650-09-M-1523. The work of T. Callaghan was partially supported by AFOSR grant FA9550-08-1-0089. The work of G. Papanicolaou was partially supported by AFOSR grant FA9550-08-1-0089 and by Air Force - SBIR FA8650-09-M-1523. We thank Elizabeth Bleszynski, Marek Bleszynski and Thomas Jaroszewicz of Monopole Research with whom we collaborated in the Air Force SBIR.

Appendices

Appendix A. The GOTCHA Volumetric SAR parameters.

The central frequency of the probing signal $f(t)$ is $\nu_0 = 9.6$Ghz and the bandwidth is $B = 622$MHz. The SAR platform trajectory is circular, at height $H = 7.3$km, with radius $R = 7.1$km and speed $V = 250$km/h or 70m/s. One circular degree of trajectory is 124m. The pulse repetition rate is 117 per degree, which means that a pulse is sent every 1.05m, and $\Delta s = 0.015$s. A typical distance to a target is $L = 10$km, and we take $|\mathbf{u}| \sim 100$km/h or 28m/sec. Then, we have from the basic image resolution theory [9], in ideal scenarios with known target motion and SAR platform trajectory, that the range resolution of the image (1.1) is $c/B = 48$cm, and the cross range resolution is $\lambda_0 L/a = 2.5$m, with one degree aperture a and central wavelength $\lambda_0 = 3$cm.

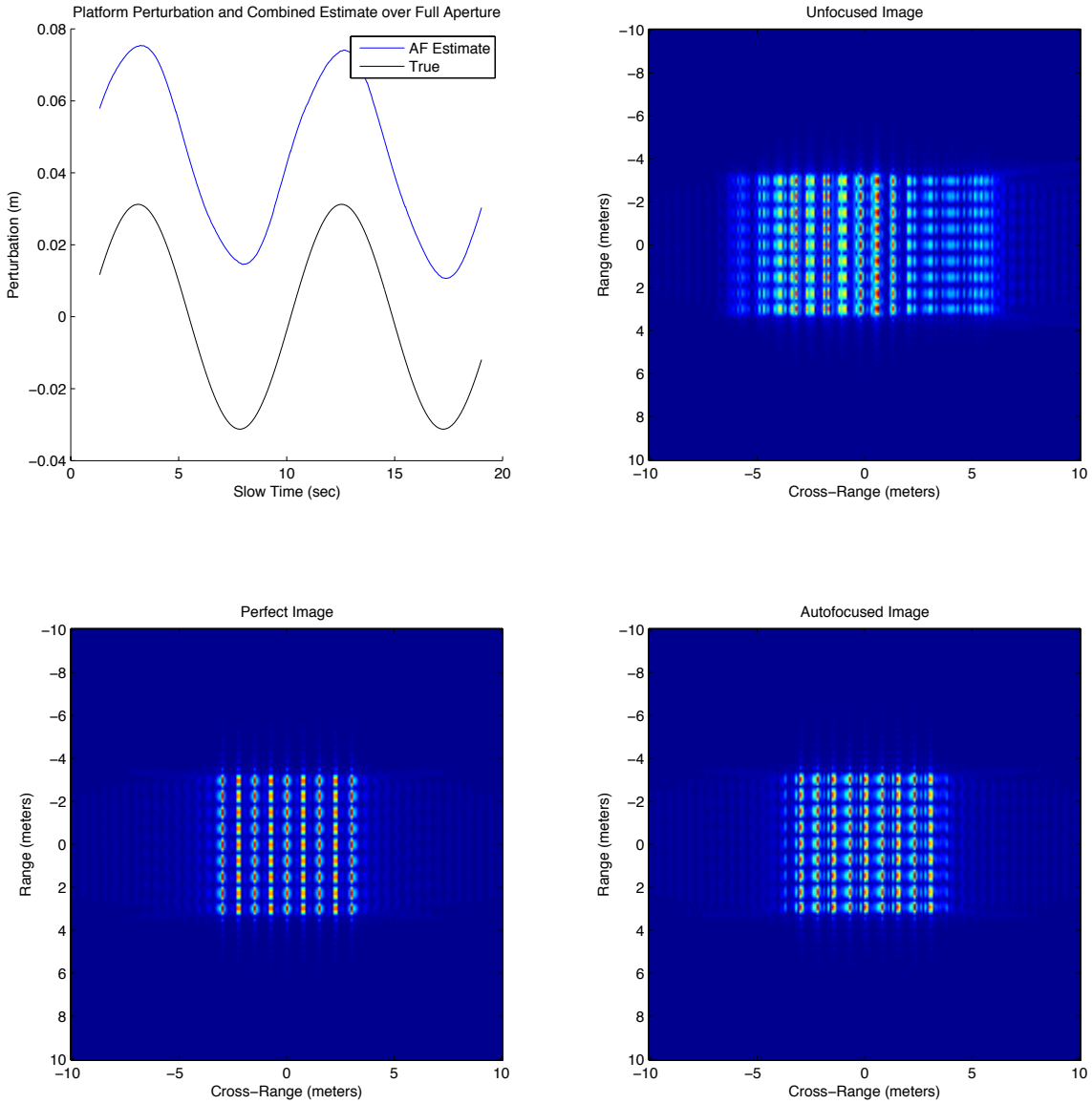

Figure 11. Autofocus of a scene with 81 stationary point scatterers. Top left: The platform trajectory perturbations along the range direction (black line) and the estimated perturbations (blue line). Bottom left: Image computed over a 1km aperture, with no platform trajectory perturbations. Top right: Unfocused image. Bottom right: Autofocused image.

Appendix B. Derivation of the data model in Proposition 1.

We begin with $D(s,t) \approx p(t, \vec{\mathbf{r}}_p(s+t))$, where $p(t,\vec{\mathbf{r}})$ is the Born approximation of the wavefield due to signal $f(t)$ emitted at $t=0$ from a point source at $\vec{\mathbf{r}}_p(s)$,

$$p(t,\vec{\mathbf{r}}) = -\int dt' \int d\mathbf{x}\, \frac{\delta(t-t'-|\vec{\mathbf{x}}-\vec{\mathbf{r}}|/c)}{4\pi|\vec{\mathbf{x}}-\vec{\mathbf{r}}|}\mathcal{R}(t',\mathbf{x})\frac{1}{c^2}\frac{\partial_t^2 f(t'-|\vec{\mathbf{x}}-\vec{\mathbf{r}}_p(s)|/c)}{4\pi|\vec{\mathbf{x}}-\vec{\mathbf{r}}_p(s)|}, \tag{B.1}$$

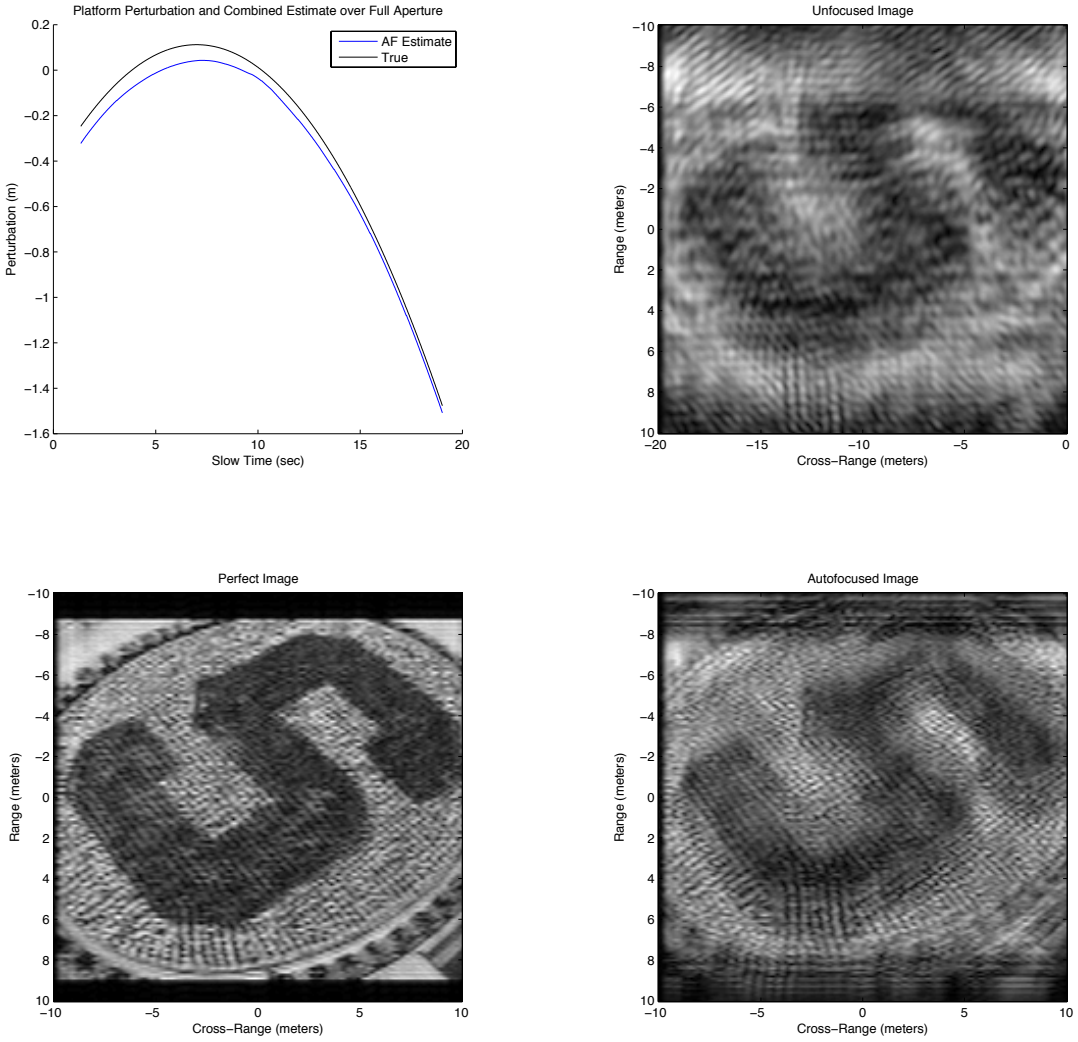

Figure 12. Autofocus of a scene created using pixel values from a low-resolution aerial picture of a garden at Stanford University. Top left: The platform trajectory perturbations along the range direction (black line) and the estimated perturbations (blue line). Bottom left: Image computed over a 1km aperture, with no platform trajectory perturbations. Top right: Unfocused image. Bottom right: Autofocused image.

where $\vec{\mathbf{x}} = (\mathbf{x}, 0)$. Using (2.2) and approximation $\vec{\mathbf{r}}_p(s+t) \approx \vec{\mathbf{r}}_p(s) + \vec{\mathbf{V}}(s)t$, we get

$$D(s,t) \approx \frac{(\omega_o/c)^2}{\left(4\pi|\vec{\mathbf{r}}_p(s) - \vec{\boldsymbol{\rho}}(s)|\right)^2} \int dt' \delta\left(t - t' - |\vec{\mathbf{r}}_p(s) + \vec{\mathbf{V}}(s)t - \vec{\boldsymbol{\rho}}(s) - \vec{\mathbf{u}}(s)t'|/c\right) \times$$
$$f\left(t' - |\vec{\mathbf{r}}_p(s) - \vec{\boldsymbol{\rho}}(s) - \vec{\mathbf{u}}(s)t'|/c\right) \tag{B.2}$$

in narrow-band regimes $\pi B \ll \omega_o$, where $\partial_t^2 f(t) \approx -\omega_o^2 f(t) = -\omega_o^2 e^{-i\omega_o t} f_B(t)$. The data model follows from (B.2) and approximations

$$|\vec{\mathbf{r}}_p(s) + \vec{\mathbf{V}}(s)t - \vec{\boldsymbol{\rho}}(s) - \vec{\mathbf{u}}(s)t'| \approx |\vec{\mathbf{r}}_p(s) - \vec{\boldsymbol{\rho}}(s)| + (t\vec{\mathbf{V}}(s) - t'\vec{\mathbf{u}}(s)) \cdot \vec{\mathbf{m}}(s),$$
$$|\vec{\mathbf{r}}_p(s) - \vec{\boldsymbol{\rho}}(s) - \vec{\mathbf{u}}(s)t'| \approx |\vec{\mathbf{r}}_p(s) - \vec{\boldsymbol{\rho}}(s)| - t'\vec{\mathbf{u}}(s) \cdot \vec{\mathbf{m}}(s),$$

with error of the order $|\vec{\mathbf{V}}(s)t|^2/L$. We obtain from the support of the δ distribution

$$t' \left[1 - \frac{\vec{\mathbf{u}}(s)}{c} \cdot \vec{\mathbf{m}}(s)\right] \approx t \left[1 - \frac{\vec{\mathbf{V}}(s)}{c} \cdot \vec{\mathbf{m}}(s)\right] - \frac{|\vec{\mathbf{r}}_p(s) - \vec{\boldsymbol{\rho}}(s)|}{c},$$

with negligible error $O\left[\frac{t^2|\vec{\mathbf{V}}|^2}{cL}\right] \ll 1$ over the interval $t \in (0, \Delta s)$. Thus,

$$D(s,t) \approx \frac{(\omega_o/c)^2}{(4\pi|\vec{\mathbf{r}}_p(s) - \vec{\boldsymbol{\rho}}(s)|)^2} f\left\{t\left[1 + \left(\frac{2\vec{\mathbf{u}}(s)}{c} - \frac{\vec{\mathbf{V}}(s)}{c}\right) \cdot \vec{\mathbf{m}}(s)\right] - \frac{2|\vec{\mathbf{r}}_p(s) - \vec{\boldsymbol{\rho}}(s)|}{c}\left[1 + \frac{\vec{\mathbf{u}}(s)}{c} \cdot \vec{\mathbf{m}}(s)\right]\right\},$$

where we neglected the error that is of the order $\frac{|\vec{\mathbf{u}}(s)|^2}{c^2} \lesssim \frac{|\vec{\mathbf{V}}(s)|^2}{c^2} \ll 1$. Now, Fourier transform in t

$$\widehat{D}(s,\omega) \approx \frac{(\omega_o/c)^2}{(4\pi|\vec{\mathbf{r}}_p(s) - \vec{\boldsymbol{\rho}}(s)|)^2} \widehat{f}_B\left[\frac{\omega}{1 + \left(2\frac{\vec{\mathbf{u}}(s)}{c} - \frac{\vec{\mathbf{V}}(s)}{c}\right) \cdot \vec{\mathbf{m}}(s)} - \omega_o\right] \exp\left\{i\omega \frac{2|\vec{\mathbf{r}}_p(s) - \vec{\boldsymbol{\rho}}(s)|}{c}\left[1 + \left(\frac{\vec{\mathbf{V}}(s)}{c} - \frac{\vec{\mathbf{u}}(s)}{c}\right) \cdot \vec{\mathbf{m}}(s)\right]\right\}, \tag{B.3}$$

and use that the support of $\widehat{f}_B$ is of order πB to write $\widehat{f}_B(\cdot) = \widehat{F}\left(\frac{\cdot}{\pi B}\right)$, with $\widehat{F}$ supported in $[-1,1]$. This implies

$$\widehat{f}_B\left[\frac{\omega}{1 + \left(2\frac{\vec{\mathbf{u}}}{c} - \frac{\vec{\mathbf{V}}}{c}\right) \cdot \vec{\mathbf{m}}} - \omega_o\right] \approx \widehat{F}\left(\frac{\omega - \omega_o}{\pi B} - \frac{\omega}{\pi B}\left(2\frac{\vec{\mathbf{u}}}{c} - \frac{\vec{\mathbf{V}}}{c}\right) \cdot \vec{\mathbf{m}}\right) \approx \widehat{f}_B(\omega - \omega_o)$$

because by (2.5),

$$\frac{\omega}{\pi B}\frac{|2\vec{\mathbf{u}} - \vec{\mathbf{V}}(s)|}{c} \sim \frac{\nu_o}{B}\frac{|\vec{\mathbf{V}}(s)|}{c} \ll 1.$$

Proposition 1 follows.

Appendix C. Proof of Proposition 2.

For a small enough time offset bound $\tilde{S}$ we can neglect $\tilde{s}$ in the amplitudes of $\widehat{D}_r\left(s \pm \frac{\tilde{s}}{2}, \omega \pm \frac{\tilde{\omega}}{2}\right)$ and obtain

$$\mathcal{W}(s, \Omega, \omega_o, T) \sim \frac{|\widehat{f}_B(0)|^4}{|\vec{\mathbf{r}}_p(s) - \vec{\boldsymbol{\rho}}(s)|^4} \int_{-2\pi B}^{2\pi B} d\tilde{\omega} \int_{-\tilde{S}}^{\tilde{S}} d\tilde{s}\, e^{i\Psi(\tilde{\omega}, \tilde{s}, s, \omega_o)},$$

with phase given by

$$\Psi(\tilde{\omega}, \tilde{s}, s, \omega_o) = \frac{2\omega_o}{c}\mathcal{T}_1(s, \tilde{s}) + \frac{\tilde{\omega}}{c}\mathcal{T}_2(s, \tilde{s}) + \tilde{s}\Omega - \tilde{\omega}T. \tag{C.1}$$

Here we let

$$\mathcal{T}_1(s, \tilde{s}) = \sum_{q=1,-1} q\left[\left|\vec{\mathbf{r}}_p\left(s + \frac{q\tilde{s}}{2}\right) - \vec{\boldsymbol{\rho}}\left(s + \frac{q\tilde{s}}{2}\right)\right| - \left|\vec{\mathbf{r}}_p\left(s + \frac{q\tilde{s}}{2}\right) - \vec{\boldsymbol{\rho}}_o\right|\right],$$

$$\mathcal{T}_2(s,\tilde{s}) = \sum_{q=1,-1}\left[\left|\vec{\mathbf{r}}_p\left(s+\frac{q\tilde{s}}{2}\right)-\vec{\boldsymbol{\rho}}\left(s+\frac{q\tilde{s}}{2}\right)\right|-\left|\vec{\mathbf{r}}_p\left(s+\frac{q\tilde{s}}{2}\right)-\vec{\boldsymbol{\rho}}_o\right|\right].$$

Now let us note that

$$\sum_{q=1,-1} q\left|\vec{\mathbf{r}}_p\left(s+\frac{q\tilde{s}}{2}\right)-\vec{\boldsymbol{\rho}}\left(s+\frac{q\tilde{s}}{2}\right)\right| \approx \tilde{s}\left(\vec{\mathbf{V}}(s)-\vec{\mathbf{u}}\right)\cdot\vec{\mathbf{m}}(s)+\frac{\tilde{s}^3}{24}\frac{d^3\left|\vec{\mathbf{r}}_p(s)-\vec{\boldsymbol{\rho}}(s)\right|}{ds^3},$$

because $\frac{d|\vec{\mathbf{r}}_p(s)-\vec{\boldsymbol{\rho}}(s)|}{ds} = \left(\vec{\mathbf{V}}(s)-\vec{\mathbf{u}}\right)\cdot\vec{\mathbf{m}}(s)$, with $\vec{\mathbf{V}}(s) = V\vec{\mathbf{t}}(s)$.

We shall assume that both $\vec{\mathbf{u}}$, and the tangential platform speed V change slowly in s. Then, the second and third derivatives of $|\vec{\mathbf{r}}_p(s)-\vec{\boldsymbol{\rho}}(s)|$ are approximated by

$$\frac{d^2\left|\vec{\mathbf{r}}_p(s)-\vec{\boldsymbol{\rho}}(s)\right|}{ds^2} \approx V\vec{\mathbf{t}}'(s)\cdot\vec{\mathbf{m}}(s)+\left(V\vec{\mathbf{t}}(s)-\vec{\mathbf{u}}\right)\cdot\vec{\mathbf{m}}'(s),$$
$$\frac{d^3\left|\vec{\mathbf{r}}_p(s)-\vec{\boldsymbol{\rho}}(s)\right|}{ds^3} \approx V\vec{\mathbf{t}}''(s)\cdot\vec{\mathbf{m}}(s)+2V\vec{\mathbf{t}}'(s)\cdot\vec{\mathbf{m}}'(s)+\left(V\vec{\mathbf{t}}(s)-\vec{\mathbf{u}}\right)\cdot\vec{\mathbf{m}}''(s)$$

and we obtain

$$\sum_{q=1,-1} q\left|\vec{\mathbf{r}}_p\left(s+\frac{q\tilde{s}}{2}\right)-\vec{\boldsymbol{\rho}}\left(s+\frac{q\tilde{s}}{2}\right)\right| \approx \tilde{s}\left(\vec{\mathbf{V}}(s)-\vec{\mathbf{u}}\right)\cdot\vec{\mathbf{m}}(s)+\frac{\tilde{s}^3}{24}\left[V\vec{\mathbf{t}}''(s)\cdot\vec{\mathbf{m}}(s)+\right.$$
$$\left.2V\vec{\mathbf{t}}'(s)\cdot\vec{\mathbf{m}}'(s)+\left(V\vec{\mathbf{t}}(s)-\vec{\mathbf{u}}\right)\cdot\vec{\mathbf{m}}''(s)\right]. \tag{C.2}$$

Similarly,

$$\sum_{q=1,-1} q\left|\vec{\mathbf{r}}_p\left(s+\frac{q\tilde{s}}{2}\right)-\vec{\boldsymbol{\rho}}_o\right| \approx \tilde{s}\vec{\mathbf{V}}(s)\cdot\vec{\mathbf{m}}_o(s)+\frac{\tilde{s}^3}{24}\left[V\vec{\mathbf{t}}''(s)\cdot\vec{\mathbf{m}}_o(s)+\right.$$
$$\left.2V\vec{\mathbf{t}}'(s)\cdot\vec{\mathbf{m}}_o'(s)+V\vec{\mathbf{t}}(s)\cdot\vec{\mathbf{m}}_o''(s)\right]. \tag{C.3}$$

Thus,

$$\frac{2\omega_o}{c}\mathcal{T}_1(s,\tilde{s}) \approx -\frac{2\omega_o\tilde{s}\vec{\mathbf{u}}}{c}\cdot\vec{\mathbf{m}}(s)+\frac{2\omega_o\tilde{s}V}{c}\,\vec{\mathbf{t}}(s)\cdot(\vec{\mathbf{m}}(s)-\vec{\mathbf{m}}_o(s))+\frac{\omega_o\tilde{s}^3V^3}{12c}\mathcal{E}_1(s), \tag{C.4}$$

with scaled remainder

$$V^2\mathcal{E}_1 = -\frac{\vec{\mathbf{u}}}{V}\cdot\vec{\mathbf{m}}''+\vec{\mathbf{t}}''\cdot[\vec{\mathbf{m}}-\vec{\mathbf{m}}_o]+2\vec{\mathbf{t}}'\cdot[\vec{\mathbf{m}}'-\vec{\mathbf{m}}_o']+\vec{\mathbf{t}}\cdot[\vec{\mathbf{m}}''-\vec{\mathbf{m}}_o'']. \tag{C.5}$$

The derivatives of $\vec{\mathbf{t}}(s)$ are determined by the differential geometry relations

$$\vec{\mathbf{t}}'(s) = -\frac{V}{R}\vec{\mathbf{n}}(s),\quad \vec{\mathbf{t}}''(s) = -\frac{V}{R}\vec{\mathbf{n}}'(s) = -\frac{V^2}{R^2}\vec{\mathbf{t}}(s), \tag{C.6}$$

with $\vec{\mathbf{n}}(s)$ the unit vector orthogonal to $\vec{\mathbf{t}}(s)$, in the flight plane defined by $\vec{\mathbf{t}}(s)$ and the center of curvature, at distance R from $\vec{\mathbf{r}}_p(s)$. The derivative of $\vec{\mathbf{m}}(s)$ is

$$\vec{\mathbf{m}}'(s) = \frac{\mathbb{P}(s)\left(V\vec{\mathbf{t}}(s)-\vec{\mathbf{u}}\right)}{|\vec{\mathbf{r}}_p(s)-\vec{\boldsymbol{\rho}}(s)|},\qquad \mathbb{P}(s) = I-\vec{\mathbf{m}}(s)\left(\vec{\mathbf{m}}(s)\right)^T, \tag{C.7}$$

and

$$\vec{\mathbf{m}}''(s) = \frac{\mathbb{P}(s)V\vec{\mathbf{t}}'(s)+\mathbb{P}'(s)\left(V\vec{\mathbf{t}}(s)-\vec{\mathbf{u}}\right)}{|\vec{\mathbf{r}}_p(s)-\vec{\boldsymbol{\rho}}(s)|}-\frac{\mathbb{P}(s)\left(V\vec{\mathbf{t}}(s)-\vec{\mathbf{u}}\right)}{|\vec{\mathbf{r}}_p(s)-\vec{\boldsymbol{\rho}}(s)|^2}\left(V\vec{\mathbf{t}}(s)-\vec{\mathbf{u}}\right)\cdot\vec{\mathbf{m}}(s)$$

is a vector orthogonal to $\vec{\mathbf{m}}'(s)$, with norm $\sim V^2/L^2$. The derivatives of $\vec{\mathbf{m}}_o(s)$ are similar. Now, we can write

$$\vec{\mathbf{m}}(s) = \vec{\mathbf{m}}_o(s)-\frac{\mathbb{P}_o(s)\left(\vec{\boldsymbol{\rho}}(s)-\vec{\boldsymbol{\rho}}_o\right)}{|\vec{\mathbf{r}}_p(s)-\vec{\boldsymbol{\rho}}_o|}+\vec{\mathcal{E}},\qquad |\vec{\mathcal{E}}| = O\left(\frac{|\vec{\boldsymbol{\rho}}(s)-\vec{\boldsymbol{\rho}}_o|^2}{L^2}\right),$$

$$|\vec{\mathbf{m}}'(s) - \vec{\mathbf{m}}_o'(s)| = O\left(\frac{u}{L}\right), \quad |\vec{\mathbf{m}}''(s) - \vec{\mathbf{m}}_o''(s)| = O\left(\frac{Vu}{L^2}\right),$$

and obtain from (C.4)

$$\frac{2\omega_o}{c}\mathcal{T}_1(s,\tilde{s}) = -\frac{2\omega_o\tilde{s}\vec{\mathbf{u}}}{c}\cdot\vec{\mathbf{m}}(s) + \frac{2\omega_o\tilde{s}V}{c}\vec{\mathbf{t}}(s)\cdot(\vec{\mathbf{m}}(s) - \vec{\mathbf{m}}_o(s)) + \frac{\omega_o\tilde{s}^3V^3}{12c}\mathcal{E}_1(s),$$

with negligible remainder $\mathcal{E}_1(s) = O\left(\frac{u}{VL^2}\right)$, when we chose the aperture $\tilde{S}V = a/2$ so that $(a/2)^3 \ll \lambda_o L^2 V/u$. This is the second assumption in (3.2).

The approximation of $\mathcal{T}_2(s,\tilde{s})$ is similar. We get

$$\sum_{q=1,-1}\left|\vec{\mathbf{r}}_p\left(s+\frac{q\tilde{s}}{2}\right) - \vec{\boldsymbol{\rho}}\left(s+\frac{q\tilde{s}}{2}\right)\right| = 2\left|\vec{\mathbf{r}}_p(s) - \vec{\boldsymbol{\rho}}(s)\right| + \frac{\tilde{s}^2}{8}\Big[V\vec{\mathbf{t}}'(s)\cdot\vec{\mathbf{m}}(s) + \Big(V\vec{\mathbf{t}}(s) - \vec{\mathbf{u}}\Big)\cdot\vec{\mathbf{m}}'(s)\Big] + O\left(\frac{\tilde{s}^4}{4!}\frac{d^4|\vec{\mathbf{r}}_p(s) - \vec{\boldsymbol{\rho}}(s)|}{ds^4}\right),$$

$$\sum_{q=1,-1}\left|\vec{\mathbf{r}}_p\left(s+\frac{q\tilde{s}}{2}\right) - \vec{\boldsymbol{\rho}}_o\right| = 2\left|\vec{\mathbf{r}}_p(s) - \vec{\boldsymbol{\rho}}_o\right| + \frac{\tilde{s}^2}{8}\Big[V\vec{\mathbf{t}}'(s)\cdot\vec{\mathbf{m}}(s) + V\vec{\mathbf{t}}(s)\cdot\vec{\mathbf{m}}'(s)\Big] + O\left(\frac{\tilde{s}^4}{4!}\frac{d^4|\vec{\mathbf{r}}_p(s) - \vec{\boldsymbol{\rho}}(s)|}{ds^4}\right),$$

aand therefore

$$\frac{\tilde{\omega}}{c}\mathcal{T}_2(s,\tilde{s}) = \frac{2\tilde{\omega}}{c}\left(|\vec{\mathbf{r}}_p(s) - \vec{\boldsymbol{\rho}}(s)| - |\vec{\mathbf{r}}_p(s) - \vec{\boldsymbol{\rho}}_o|\right) + \frac{\tilde{\omega}\tilde{s}^2}{8c}\mathcal{E}_2(s,\tilde{s}), \tag{C.8}$$

with scaled remainder

$$\mathcal{E}_2(s,\tilde{s}) = O\left(\frac{V^2|\vec{\boldsymbol{\rho}}(s) - \vec{\boldsymbol{\rho}}_o|}{L^2}\right) + O\left(\frac{Vu}{L}\right), \tag{C.9}$$

that can be neglected if $\frac{(a/2)^2}{\lambda_o L} \ll \frac{\nu_o V}{Bu}$. This is the first assumption in (3.2). Note that the other term in the remainder $\mathcal{E}_2$ is small because

$$\frac{\tilde{\omega}\tilde{s}^2V^2|\vec{\boldsymbol{\rho}}(s) - \vec{\boldsymbol{\rho}}_o|}{c|\vec{\mathbf{r}}_p(s) - \vec{\boldsymbol{\rho}}_o|^2} \sim \frac{B}{\nu_o}\frac{(a/2)^2}{\lambda_o L}\frac{|\vec{\boldsymbol{\rho}}(s) - \vec{\boldsymbol{\rho}}_o|}{L} \ll \frac{V}{u}\frac{|\vec{\boldsymbol{\rho}}(s) - \vec{\boldsymbol{\rho}}_o|}{L} \ll 1.$$

Gathering all the results we obtain the phase approximation

$$\Psi \approx \tilde{s}\omega_o\left[\frac{\Omega}{\omega_o} - \frac{2\vec{\mathbf{u}}}{c}\cdot\vec{\mathbf{m}}(s) + \frac{2V}{c}\vec{\mathbf{t}}(s)\cdot(\vec{\mathbf{m}}(s) - \vec{\mathbf{m}}_o(s))\right] + \tilde{\omega}\left[\tau(s,\vec{\boldsymbol{\rho}}(s)) - \tau(s,\vec{\boldsymbol{\rho}}_o) - T\right],$$

and Proposition 2 follows after substituting Ψ in the expression of the Wigner transform $\mathcal{W}(s,\Omega,\omega_o,T)$, and integrating over $\tilde{s}$ and $\tilde{\omega}$.

When we relax the first assumption in (3.2) to (3.6), the remainder $\mathcal{E}_2$ in (C.8) is no longer negligible, and we obtain a Fresnel integral in $\tilde{s}$. The method of stationary phase [5] tells us that the quadratic term in (C.8) does not affect the location of the peak of this integral, which is the information used in the target motion estimation.

Appendix D. Proof of Proposition 4.

The perturbation of the phase Ψ of the Wigner transform of the range compressed data is given by

$$\delta\Psi(\tilde{\omega},\tilde{s},s,\omega_o) = \frac{2\omega_o}{c}\delta\mathcal{T}_1(s,\tilde{s}) + \frac{\tilde{\omega}}{c}\delta\mathcal{T}_2(s,\tilde{s}), \tag{D.1}$$

where

$$\delta\mathcal{T}_1 = \sum_{q=1,-1} q\left[\left|\vec{\mathbf{r}}_p\Big(s+\frac{q\tilde{s}}{2}\Big)+\vec{\boldsymbol{\mu}}\Big(s+\frac{q\tilde{s}}{2}\Big)-\vec{\boldsymbol{\rho}}\Big(s+\frac{q\tilde{s}}{2}\Big)\right|-\left|\vec{\mathbf{r}}_p\Big(s+\frac{q\tilde{s}}{2}\Big)-\vec{\boldsymbol{\rho}}\Big(s+\frac{q\tilde{s}}{2}\Big)\right|\right]$$

$$\delta\mathcal{T}_2 = \sum_{q=1,-1}\left[\left|\vec{\mathbf{r}}_p\Big(s+\frac{q\tilde{s}}{2}\Big)+\vec{\boldsymbol{\mu}}\Big(s+\frac{q\tilde{s}}{2}\Big)-\vec{\boldsymbol{\rho}}\Big(s+\frac{q\tilde{s}}{2}\Big)\right|-\left|\vec{\mathbf{r}}_p\Big(s+\frac{q\tilde{s}}{2}\Big)-\vec{\boldsymbol{\rho}}\Big(s+\frac{q\tilde{s}}{2}\Big)\right|\right].$$

Proceeding as in Appendix C, we write

$$\delta\mathcal{T}_1(s,\tilde{s}) \approx \tilde{s}\left(V\vec{\mathbf{t}}(s)+\vec{\boldsymbol{\mu}}'(s)-\vec{\mathbf{u}}\right)\cdot\vec{\mathbf{m}}_\mu(s)-\tilde{s}\left(V\vec{\mathbf{t}}(s)-\vec{\mathbf{u}}\right)\cdot\vec{\mathbf{m}}(s)+ \frac{\tilde{s}^3}{24}\left|\frac{d^3\left[\vec{\mathbf{r}}_p(s)+\vec{\boldsymbol{\mu}}(s)-\vec{\boldsymbol{\rho}}(s)\right|}{ds^3}-\frac{d^3\left|\vec{\mathbf{r}}_p(s)-\vec{\boldsymbol{\rho}}(s)\right|}{ds^3}\right],$$

where

$$\vec{\mathbf{m}}_\mu(s)=\frac{\vec{\mathbf{r}}_p(s)+\vec{\boldsymbol{\mu}}(s)-\vec{\boldsymbol{\rho}}(s)}{|\vec{\mathbf{r}}_p(s)+\vec{\boldsymbol{\mu}}(s)-\vec{\boldsymbol{\rho}}(s)|}=\vec{\mathbf{m}}(s)+\frac{\mathbb{P}(s)\vec{\boldsymbol{\mu}}(s)}{|\vec{\mathbf{r}}_p(s)-\vec{\boldsymbol{\rho}}(s)|}+\vec{\mathcal{E}},\quad |\vec{\mathcal{E}}|=O\Big(\frac{|\vec{\boldsymbol{\mu}}(s)|^2}{|\vec{\mathbf{r}}_p(s)-\vec{\boldsymbol{\rho}}_\star|^2}\Big) \tag{D.2}$$

and

$$\frac{d^2\left|\vec{\mathbf{r}}_p(s)+\vec{\boldsymbol{\mu}}(s)-\vec{\boldsymbol{\rho}}(s)\right|}{ds^2}=\left(V\vec{\mathbf{t}}'(s)+\vec{\boldsymbol{\mu}}''(s)\right)\cdot\vec{\mathbf{m}}_\mu(s)+\left(V\vec{\mathbf{t}}(s)+\vec{\boldsymbol{\mu}}'(s)-\vec{\mathbf{u}}\right)\cdot\vec{\mathbf{m}}'_\mu(s).$$

Here

$$\vec{\mathbf{m}}'_\mu(s)=\frac{\mathbb{P}_\mu\left(V\vec{\mathbf{t}}(s)+\vec{\boldsymbol{\mu}}'(s)-\vec{\mathbf{u}}\right)}{|\vec{\mathbf{r}}_p(s)+\vec{\boldsymbol{\mu}}(s)-\vec{\boldsymbol{\rho}}(s)|},\qquad \mathbb{P}_\mu(s)=I-\vec{\mathbf{m}}_\mu(s)\left(\vec{\mathbf{m}}_\mu(s)\right)^T, \tag{D.3}$$

and furthermore,

$$\frac{d^3\left|\vec{\mathbf{r}}_p(s)+\vec{\boldsymbol{\mu}}(s)-\vec{\boldsymbol{\rho}}(s)\right|}{ds^3}\approx\left(V\vec{\mathbf{t}}''(s)+\vec{\boldsymbol{\mu}}'''(s)\right)\cdot\vec{\mathbf{m}}_\mu(s)+2\left(V\vec{\mathbf{t}}'(s)+\vec{\boldsymbol{\mu}}''(s)\right)\cdot\vec{\mathbf{m}}'_\mu(s)+ \left(V\vec{\mathbf{t}}(s)+\vec{\boldsymbol{\mu}}'(s)-\vec{\mathbf{u}}\right)\cdot\vec{\mathbf{m}}''_\mu(s). \tag{D.4}$$

The second derivative of $\vec{\mathbf{m}}_\mu(s)$ follows by differentiation in (D.3) and it satisfies

$$\left|\vec{\mathbf{m}}''_\mu(s)\right|=O\left(\frac{V^2}{L^2}\right)+O\left(\frac{\left|\vec{\boldsymbol{\mu}}''(s)\right|}{L}\right), \tag{D.5}$$

because $|\vec{\boldsymbol{\mu}}'(s)|\ll V$. This gives

$$\frac{2\omega_o\tilde{s}}{c}\delta\mathcal{T}_1=\frac{2\omega_o\tilde{s}}{c}\vec{\boldsymbol{\mu}}'(s)\cdot\vec{\mathbf{m}}(s)+\frac{2\omega_o\tilde{s}V}{c}\left(\vec{\mathbf{t}}(s)-\frac{\vec{\mathbf{u}}}{V}\right)\cdot\frac{\mathbb{P}\vec{\boldsymbol{\mu}}(s)}{|\vec{\mathbf{r}}_p(s)-\vec{\boldsymbol{\rho}}(s)|}+\frac{\omega_oV\tilde{s}}{c}\mathcal{E}_4(s),$$

with scaled remainder

$$\frac{\omega_oV\tilde{s}}{c}\mathcal{E}_4(s)=O\left[\frac{\omega_o}{c}\frac{a\vec{\boldsymbol{\mu}}'}{V}\cdot\frac{\mathbb{P}\vec{\boldsymbol{\mu}}}{L}+\frac{a|\vec{\boldsymbol{\mu}}|^2}{\lambda_oL^2}+\frac{a^3}{\lambda_oL^2}+\frac{a}{\lambda_oL}\frac{a^2|\vec{\boldsymbol{\mu}}''|}{V^2}+\frac{a^3|\vec{\boldsymbol{\mu}}'''\cdot\vec{\mathbf{m}}_\mu|}{V^3\lambda_o}\right].$$

The first term in the remainder is negligible by (3.21),

$$\frac{\omega_o}{c}\frac{a}{V}\vec{\boldsymbol{\mu}}'(s)\cdot\frac{\mathbb{P}(s)\vec{\boldsymbol{\mu}}(s)}{L}\sim\frac{1}{\lambda_o}\frac{\lambda_oL}{a\delta}\frac{\overline{\mu}}{L}=\frac{\overline{\mu}}{a\delta}\ll 1.$$

The second term is negligible because

$$\frac{a|\vec{\boldsymbol{\mu}}(s)|^2}{\lambda_oL^2}\sim\frac{\overline{\mu}^2}{a^2}\frac{a^3}{\lambda_oL^2}\ll 1,$$

by (3.2) and $u\lesssim V$, and the fourth term is negligible by assumption (3.22)

$$\frac{a^2|\vec{\boldsymbol{\mu}}''(s)|}{V^2}\sim\frac{\lambda_o}{\gamma},$$

for all $\gamma \gg a/L$, not only $\gamma \sim \delta$, as assumed in (3.30). Finally, the last term in the remainder is negligible by assumption (3.23).

We have now shown that

$$\frac{2\omega_o \tilde{s}}{c}\delta\mathcal{T}_1(s,\tilde{s}) \approx \frac{2\omega_o \tilde{s}}{c}\vec{\boldsymbol{\mu}}'(s)\cdot\vec{\mathbf{m}}(s) + \frac{2\omega_o \tilde{s}V}{c}\left(\vec{\mathbf{t}}(s) - \frac{\vec{\mathbf{u}}}{V}\right)\cdot\frac{\mathbb{P}(s)\vec{\boldsymbol{\mu}}(s)}{|\vec{\mathbf{r}}_p(s) - \vec{\boldsymbol{\rho}}(s)|}. \tag{D.6}$$

Similarly, we get

$$\frac{\tilde{\omega}}{c}\delta\mathcal{T}_2(s,\tilde{s}) = \frac{2\tilde{\omega}}{c}\vec{\boldsymbol{\mu}}(s)\cdot\vec{\mathbf{m}}(s) + \mathcal{E}_5(s,\tilde{s}) \tag{D.7}$$

with remainder

$$\mathcal{E}_5(s,\tilde{s}) = O\left(\frac{\tilde{\omega}}{c}\frac{\overline{\mu}^2}{L}\right) + O\left(\frac{\tilde{\omega}}{c}\frac{a^2}{V^2}\left[\frac{d^2|\vec{\mathbf{r}}_p(s) + \vec{\boldsymbol{\mu}}(s) - \vec{\boldsymbol{\rho}}(s)|}{ds^2} - \frac{d^2|\vec{\mathbf{r}}_p(s) - \vec{\boldsymbol{\rho}}(s)|}{ds^2}\right]\right).$$

The first term in this remainder is negligible by (3.2) and the assumption $|\vec{\boldsymbol{\mu}}| \sim \overline{\mu} \ll a$. Note that the second term in $\mathcal{E}_5$ is similar to the remainder $\mathcal{E}_2$ estimated in Appendix C, and that all terms but

$$\frac{\tilde{\omega}}{c}\frac{a^2}{V^2}\vec{\boldsymbol{\mu}}''(s)\cdot\vec{\mathbf{m}}_\mu(s) \sim \frac{B}{\nu_o\gamma}$$

are negligible under our assumptions. Therefore, we get

$$\frac{\tilde{\omega}}{c}\delta\mathcal{T}_2(s,\tilde{s}) \approx \frac{2\tilde{\omega}}{c}\vec{\boldsymbol{\mu}}(s)\cdot\vec{\mathbf{m}}(s) + \frac{\tilde{\omega}}{c}\frac{\tilde{s}^2}{2}\vec{\boldsymbol{\mu}}''(s)\cdot\vec{\mathbf{m}}_\mu(s) \tag{D.8}$$

and the perturbation of the phase in the Wigner transform is given by

$$\delta\Psi(\tilde{\omega},\tilde{s},s,\omega_o) \approx \frac{2\omega_o\tilde{s}V}{c}\left[\frac{1}{V}\vec{\boldsymbol{\mu}}'(s)\cdot\vec{\mathbf{m}}(s) + \left(\vec{\mathbf{t}}(s) - \frac{\vec{\mathbf{u}}}{V}\right)\cdot\frac{\mathbb{P}(s)\vec{\boldsymbol{\mu}}(s)}{|\vec{\mathbf{r}}_p(s) - \vec{\boldsymbol{\rho}}(s)|}\right] + \frac{2\tilde{\omega}}{c}\vec{\boldsymbol{\mu}}(s)\cdot\vec{\mathbf{m}}(s) + \frac{\tilde{\omega}}{c}\frac{\tilde{s}^2}{2}\vec{\boldsymbol{\mu}}''(s)\cdot\vec{\mathbf{m}}_\mu(s). \tag{D.9}$$

The last term in $\delta\Psi$ is of order $B/(\nu_o\gamma)$, and can be neglected when $\gamma \sim \delta \gg B/\nu_o$. Equation (3.26) follows after introducing the phase (D.9) in the Wigner transform and integrating in $\tilde{s}$ and $\tilde{\omega}$.

When $\gamma \lesssim B/\nu_o$, we obtain a more complicated expression of $\mathcal{W}$, involving a Fresnel integral in $\tilde{s}$. However, the quadratic phase $\frac{\tilde{\omega}}{c}\frac{\tilde{s}^2}{2}\vec{\boldsymbol{\mu}}''(s)\cdot\vec{\mathbf{m}}_\mu(s)$ does not affect the location of the peak of the resulting integral in $\tilde{s}$ [1], which means that the velocity estimation described in Section 3.4.2 should work for $\gamma \lesssim B/\nu_o$, as well.

The derivation of equation (3.27) is similar, and we do not include it here.

References

[1] Milton Abramowitz and Irene A. Stegun. *Handbook of mathematical functions with formulas, graphs, and mathematical tables*. Dover, New York, 1972.

[2] S. Barbarossa. New autofocusing technique for SAR images based on the Wigner-Ville distribution. *ELECTRONICS LETTERS*, 26(18):1533–1534, 1990.

[3] S. Barbarossa and A. Farina. Detection and imaging of moving objects with synthetic aperture radar. *IEE Proceedings-F*, 139(1):79–88, 1992.

[4] S. Barbarossa and A. Scaglione. Autofocusing of SAR images based on the product of high-order ambiguity function. *IEE Proc.-Radar, Sonar Navig.*, 145(5):269–273, 1998.

[5] C. M. Bender and S. A. Orszag. *Advanced mathematical methods for scientists and engineers*. McGraw-Hill, Inc, 1978.

[6] G. Beylkin. Imaging of discontinuities in the inverse scattering problem by inversion of a causal generalized Radon transform. *J. Math. Phys.*, 26(1):99–108, 1985.

[7] C.H. Casteel Jr, L.R.A. Gorham, M.J. Minardi, S.M. Scarborough, K.D. Naidu, and U.K. Majumder. A challenge problem for 2d/3d imaging of targets from a volumetric data set in an urban environment. In *Proceedings of SPIE*, volume 6568, page 65680D, 2007.

[8] M. Cheney. A mathematical tutorial on synthetic aperture radar. *SIAM review*, 43(2):301–312, 2001.

[9] John C. Curlander and Robert N. McDonough. *Synthetic Aperture Radar: Systems and Signal Processing*. Wiley-Interscience, 1991.

[10] Y. Ding and DC Munson Jr. Time-frequency methods in SAR imaging of moving targets. In *IEEE International Conference on Acoustics, Speech, and Signal Processing, 2002. Proceedings.(ICASSP'02)*, volume 3, 2002.

[11] Y. Ding, N. Xue, and DC Munson Jr. An analysis of time-frequency methods in SAR imaging of movingtargets. In *Sensor Array and Multichannel Signal Processing Workshop. 2000. Proceedings of the 2000 IEEE*, pages 221–225, 2000.

[12] C.V. Jakowatz, Jr and D.E. Wahl. Eigenvector method for maximum-likelihood estimation of phase errors in synthetic-aperture-radar imagery. *Journal of the Optical Society of America A*, 10(12):2539–2546, 1993.

[13] Charles V. Jakowatz Jr., Daniel E. Wahl, Paul H. Eichel, Dennis C. Ghiglia, and Paul A. Thompson. *Spotlight-mode synthetic aperture radar: A signal processing approach*. Springer, New York, NY, 1996.

[14] R.L. Morrison, M.N. Do, and D.C. Munson. SAR image autofocus by sharpness optimization: A theoretical study. *IEEE Transactions on Image Processing*, 16(9):2309, 2007.

[15] F. Natterer and F. Wübbeling. *Mathematical methods in image reconstruction*. Society for Industrial and Applied Mathematics, 2001.

[16] T. Sparr. Time-Frequency Signatures of a Moving Target in SAR Images. Paper presented at the RTO SET Symposium on Target Identification and Recognition Using RF Systems, Oslo, Norway, 11-13 October, 2004. Published in RTO-MP-SET-080.

[17] T. Sparr. Comparison of quadratic time-frequency methods applied to ISAR imaging of aircraft. In *Proceedings of SPIE*, volume 4738, page 279, 2002.